PNAS RESEARCH ARTICLE | CELL BIOLOGY

AMBRA1 levels predict resistance to MAPK inhibitors in melanoma

Luca Di Leo[a], Chiara Pagliuca[a], Ali Kishk[b], Salvatore Rizza[c], Christina Tsiavou[a], Chiara Pecorari[c], Christina Dahl[d], Maria Pires Pacheco[b], Rikke Tholstrup[e], Jonathan Richard Brewer[e], Pietro Berico[f], Eva Hernando[f], Francesco Cecconi[g,h], Robert Ballotti[i,j], Corine Bertolotto[i,j], Giuseppe Filomeni[c], Morten Frier Gjerstorff[k,l], Thomas Sauter[b], Penny Lovat[m], Per Guldberg[d,k], and Daniela De Zio[a,k,1]

Affiliations are included on p. 12.

Edited by M. Celeste Simon, University of Pennsylvania Perelman School of Medicine, Philadelphia, PA; received January 16, 2024; accepted May 20, 2024

Intrinsic and acquired resistance to mitogen-activated protein kinase inhibitors (MAPKi) in melanoma remains a major therapeutic challenge. Here, we show that the clinical development of resistance to MAPKi is associated with reduced tumor expression of the melanoma suppressor Autophagy and Beclin 1 Regulator 1 (AMBRA1) and that lower expression levels of AMBRA1 predict a poor response to MAPKi treatment. Functional analyses show that loss of AMBRA1 induces phenotype switching and orchestrates an extracellular signal-regulated kinase (ERK)-independent resistance mechanism by activating focal adhesion kinase 1 (FAK1). In both in vitro and in vivo settings, melanomas with low AMBRA1 expression exhibit intrinsic resistance to MAPKi therapy but higher sensitivity to FAK1 inhibition. Finally, we show that the rapid development of resistance in initially MAPKi-sensitive melanomas can be attributed to preexisting subclones characterized by low AMBRA1 expression and that cotreatment with MAPKi and FAK1 inhibitors (FAKi) effectively prevents the development of resistance in these tumors. In summary, our findings underscore the value of AMBRA1 expression for predicting melanoma response to MAPKi and supporting the therapeutic efficacy of FAKi to overcome MAPKi-induced resistance.

AMBRA1 | melanoma | targeted therapy | MAPK inhibitors | FAK1

Cutaneous melanoma, a malignancy arising from melanocytes, is a highly aggressive variant of skin cancer with the potential to metastasize to various anatomical sites in the absence of timely detection and intervention (1, 2). Common genetic abnormalities in melanoma include mutations in the v-raf murine sarcoma viral oncogene homolog B1 (BRAF), the neuroblastoma RAS viral oncogene homolog (NRAS), the cyclin-dependent kinase inhibitor 2A (CDKN2A), and the phosphatase and tensin homolog (PTEN) (1, 2). These abnormalities lead to hyperactivation of the mitogen-activated protein kinase (MAPK) and phosphatidylinositol 3-kinase/protein kinase B (AKT) signaling pathways, which are both essential to promoting cellular growth (3). Pharmaceutical agents targeting these pathways have shown remarkable efficacy in clinical trials, resulting in United States Food and Drug Administration (FDA) approval of several drugs for melanoma treatment (4–10), including inhibitors of the MAPK inhibitors pathway (MAPKi), such as the BRAF inhibitors (BRAFi) vemurafenib and dabrafenib and the MAPK kinase inhibitor (MEKi) trametinib (4–10). Targeted therapy using these drugs provides a more precise and effective approach for $BRAF^{V600E}$-mutated melanoma when compared with traditional chemotherapy (1–3, 8, 11, 12). However, the therapeutic challenge of eradicating late-stage melanoma persists due to the emergence of resistance mechanisms to MAPKi (1, 8, 13).

Resistance to MAPKi in melanoma may manifest as intrinsic (primary) resistance, arising initially, or as acquired resistance, which develops over time. Intrinsic resistance is attributed to various factors, including genetic changes (12–14). Alternatively, acquired resistance often results from a combination of evolutionary processes and the tumoral adaptive response to treatment, leading to a transition to drug-resistant states (12–14). Phenotype switching, a phenomenon recently recognized among the hallmarks of cancer (15), plays a pivotal role in melanoma resistance to MAPK-targeted therapy (16–19). This involves reversible transcriptional changes and epigenetic modifications (18), enabling dynamic transitions between proliferative/melanocytic and invasive/undifferentiated or drug-resistant states (16–19).

In recent years, the functional landscape of Autophagy and Beclin 1 Regulator 1 (AMBRA1) has expanded beyond its established role as an autophagy regulator (20, 21). Increasingly intertwined with cancer biology, particularly in the context of the cutaneous microenvironment and epidermal differentiation, AMBRA1 has been implicated in regulating cell proliferation and invasion (20, 22–27). Our previous work has unveiled that AMBRA1 deficiency promotes melanoma formation, enhances the invasive phenotype (25), and modifies the

Significance

The use of mitogen-activated protein kinase inhibitors (MAPKi) in the treatment of melanoma remains a clinical challenge due to preexistence or development of therapy resistance. Genetic changes or tumoral evolutionary processes have been documented as mechanisms coordinating this phenomenon. Previous evidence indicates that loss of Autophagy and Beclin 1 Regulator 1 (AMBRA1) promotes melanoma proliferation and invasion. Here, we show the clinical implications of AMBRA1 expression levels as predictive of intrinsic and acquired MAPKi resistance in melanoma. Moreover, we identify AMBRA1-dependent focal adhesion kinase 1 (FAK1) activation as a therapeutic target to counteract MAPKi resistance in melanoma.

Author contributions: L.D.L. and D.D.Z. designed research; L.D.L., C. Pagliuca, A.K., S.R., C.T., C. Pecorari, R.T., and P.B. performed research; C.D., M.P.P., P.B., E.H., F.C., M.F.G., P.L., P.G., and D.D.Z. contributed new reagents/analytic tools; L.D.L., A.K., S.R., C.T., C. Pecorari, R.T., J.R.B., P.B., R.B., C.B., T.S., and D.D.Z. analyzed data; and L.D.L., G.F., P.G., and D.D.Z. wrote the paper.

Competing interest statement: P.L. is Chief Scientific Officer for AMLo Biosciences Ltd.

This article is a PNAS Direct Submission.

[1]To whom correspondence may be addressed. Email: dzio@cancer.dk.

This article contains supporting information online at https://www.pnas.org/lookup/suppl/doi:10.1073/pnas.2400566121/-/DCSupplemental.

Published June 13, 2024.

tumor immune microenvironment in preclinical models of melanoma (28). Additionally, specific *AMBRA1* missense mutations have been linked to an increased tumorigenic potential in human melanoma cells (29), reinforcing the notion that AMBRA1 acts as a bona fide tumor suppressor in melanoma.

This study significantly expands our investigation into the effects of AMBRA1 deficiency in melanoma biology, with a specific focus on its implications for resistance to BRAFi/MEKi therapy and phenotype switching. Our ultimate goal is to identify vulnerable targets that can be exploited to overcome MAPKi resistance in melanoma.

Results

AMBRA1 Expression Is Down-Regulated in MAPKi-Resistant Melanoma. To explore the possible role of AMBRA1 in melanoma response to MAPKi treatment, we assessed *AMBRA1* expression in two cohorts of metastatic melanoma patients [GSE50509 (30) and GSE65185 (31)], pretreatment (baseline) and after treatment (resistant) with MAPKi. This analysis revealed a downregulation of AMBRA1 upon therapy resistance in ~32% of the cases across both cohorts (Fig. 1*A*). Consistently, *AMBRA1* expression was downregulated in BRAFi posttreatment samples in a cohort of melanoma patient-derived xenografts (PDXs) [GSE129127 (32)] (Fig. 1*B*) and in an established PDX model (MEL006) of minimal residual disease (33) (*SI Appendix*, Fig. S1*A*). By using a 25% cut-off, we categorized baseline samples from the GSE50509 and GSE65185 cohorts into AMBRA1^{HIGH} (upper quartile) and AMBRA1^{LOW} (lower quartile) groups (Fig. 1*C*). Notably, the significant reduction in AMBRA1 expression in MAPKi-resistant samples was observed solely in the AMBRA1^{HIGH} baseline group (Fig. 1*D*).

We next employed human melanoma cell lines ranked for AMBRA1 protein expression, among which we selected FM-93/2 (AMBRA1^{HIGH}) and M24 (AMBRA1^{LOW}) as representative cell lines for our initial investigation of resistance development (*SI Appendix*, Fig. S1*B*). Following chronic exposure to BRAFi, we observed a significant reduction in AMBRA1 protein levels in all FM-93/2-derived BRAFi-resistant cell lines (R1 to R4) compared to the sensitive line (S) (Fig. 1*E*). Conversely, no major differences in AMBRA1 expression were observed in R1-R4 vs. S in the M24 cell line (Fig. 1*E*). Extending the analysis to other AMBRA1^{LOW} (FM-55/M2, Mel-5392, and OCM-3; *SI Appendix*, Fig. S1*C*) and AMBRA1^{HIGH} (M17, M88, and Ma-Mel-51; *SI Appendix*, Fig. S1*D*) cell lines, we observed a ~67% reduction in the AMBRA1 expression ratio across all resistant and sensitive cells (Fig. 1 *F* and *G*). Evaluation of AMBRA1 expression in paired resistant and sensitive cell lines mirrored the cohort results (Fig. 1 *A* and *D*), with significant differences for AMBRA1 downregulation observed only in the AMBRA1^{HIGH} group (Fig. 1*H*). Notably, AMBRA1^{LOW} cells required shorter time for the establishment of resistant cell lines, when compared with AMBRA1^{HIGH} cells (*SI Appendix*, Fig. S1*E*). Chronic exposure to BRAFi in murine YUMM1.7 and YUMM1.1 melanoma cell lines

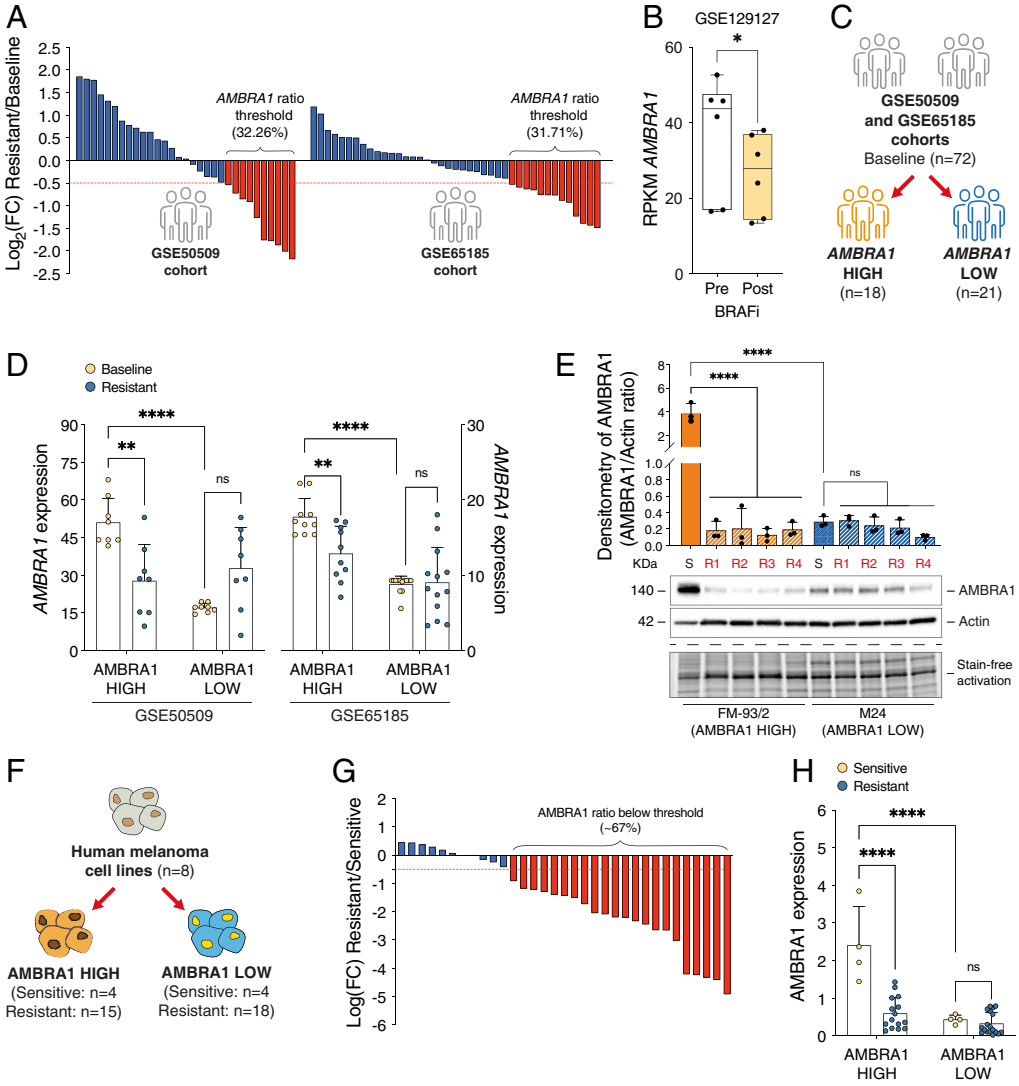

Fig. 1. AMBRA1 downregulation upon resistance to MAPKi. (*A*) Waterfall plot of Log(FC) (FC = fold change) ratio of *AMBRA1* expression between MAPKi-resistant and baseline (pretreatment) tumors in GSE50509 and GSE65185 cohorts (n = 72). The red line indicates cut-off. (*B*) *AMBRA1* expression in BRAFi (vemurafenib)-treated (Post; n = 6) and pretreatment (Pre; n = 6) PDX tumors from GSE129127 (Unpaired *t* test; **P* = 0.021). (*C*) Baseline tumors from GSE50509 and GSE65185 cohorts were ranked as AMBRA1^{HIGH} (n = 18) and AMBRA1^{LOW} (n = 21) and (*D*) modulation of *AMBRA1* expression analyzed in matching resistant tumors. Each dot represents a sample. GSE50509: n = 8/group; 2-way ANOVA; ***P* = 0.0031; *****P* < 0.0001. GSE65185: AMBRA1^{HIGH} baseline n = 10; AMBRA1^{HIGH} resistant n = 10; AMBRA1^{LOW} baseline n = 13; AMBRA1^{LOW} resistant n = 13; 2-way ANOVA; ***P* = 0.0078; *****P* < 0.0001. (*E*) Representative western blot (n = 4) of AMBRA1 in sensitive (S) and vemurafenib-resistant (R1 to R4) cell lines from the AMBRA1^{HIGH} FM-93/2 and AMBRA1^{LOW} M24 cell lines. Densitometry of AMBRA1 is shown as ratio on Actin ±SD (2-way ANOVA; *****P* < 0.0001). (*F*) BRAF^{V600E}-mutated ESTDAB cells have been ranked as AMBRA1^{HIGH} (n = 4) and AMBRA1^{LOW} (n = 4), vemurafenib-resistant cells generated and (*G*) AMBRA1 expression analyzed and shown as in *A* (n = 33). The red line indicates cut-off. (*H*) Changes in AMBRA1 levels are shown between vemurafenib-resistant and matching sensitive cell lines for AMBRA1^{HIGH} and AMBRA1^{LOW} cells. Each dot represents a cell line (AMBRA1^{HIGH}: sensitive n = 4; resistant n = 15. AMBRA1^{LOW}: sensitive n = 4; resistant n = 18) (2-way ANOVA; *****P* < 0.0001). ns = not significant.

also resulted in a significant loss of Ambra1 expression (*SI Appendix*, Fig. S1*F*). Following a 7-d depletion of BRAFi, AMBRA1 protein levels were not rescued in either FM-93/2 (*SI Appendix*, Fig. S1*G*) or YUMM1.7 (*SI Appendix*, Fig. S1*H*) BRAFi-resistant cells.

Collectively, these findings indicate a widespread downregulation of AMBRA1 expression upon the acquisition of resistance to MAPKi therapy in melanoma.

AMBRA1 Expression Levels Correlate with Response to MAPKi. We next sought to assess the correlation between AMBRA1 protein expression levels and response to MAPKi in melanoma cell lines. By utilizing the primary PRISM database, BRAF-mutated cell lines (V600E or V600K; *SI Appendix*, Fig. S2*A*) with different AMBRA1 levels (*SI Appendix*, Fig. S2*B*) were screened for individual MAPKi sensitivity (Fig. 2*A*). Results were first visualized using a heatmap (*SI Appendix*, Fig. S2*C*) and then represented as a linear model fitted between the median drug scores and AMBRA1 protein levels for each cell line (*SI Appendix*, Fig. S2*D*). Overall, this comprehensive analysis indicates that AMBRA1 expression negatively correlates with response to MAPKi (Fig. 2*B*). The MEKi cobimetinib exhibited the strongest negative correlation with AMBRA1 expression levels (R^2 = 0.42 and P = 0.0027) (Fig. 2*B*).

Extending this analysis in vitro using the panel of $BRAF^{V600E}$-mutated $AMBRA1^{HIGH}$ and $AMBRA1^{LOW}$ melanoma cell lines, we evaluated cell viability following acute treatment with increasing doses of BRAFi or MEKi (Fig. 2 *C* and *D*). The resistance index to either drug, calculated as the ratio between percentage of survival of MAPKi-treated and -untreated cells, revealed that $AMBRA1^{LOW}$ cells exhibited a higher resistance to both BRAFi and MEKi compared with $AMBRA1^{HIGH}$ cells (Fig. 2*E*). Further analysis determining EC_{50} values for both drugs in each cell line (Fig. 2*F*) and plotting them against AMBRA1 protein levels (*SI Appendix*, Fig. S1*B*) confirmed a negative correlation with AMBRA1 expression for both BRAFi (r = –0.9513; P = 0.0003) (Fig. 2*G*) and MEKi (r = –0.8816; P = 0.0038) (Fig. 2*H*).

Altogether, these results suggest that low levels of AMBRA1 are associated with BRAFi/MEKi resistance.

Modulation of AMBRA1 Levels Affects Response to MAPKi. Next, we genetically manipulated AMBRA1 in melanoma cells to investigate its impact on MAPKi response. Transfection with a plasmid encoding AMBRA1 in the $AMBRA1^{LOW}$ M24 cells followed by BRAFi treatment (Fig. 3*A*) and in FM-93/2- (*SI Appendix*, Fig. S3*A*) and M17-derived (*SI Appendix*, Fig. S3*B*) BRAFi-resistant cells demonstrated a significant resensitization to BRAFi (Fig. 3 *B* and *C* and *SI Appendix*, Fig. S3 *A* and *B*). Conversely, $AMBRA1^{HIGH}$ FM-93/2 cells transfected with a siRNA targeting AMBRA1 (siAMBRA1) (Fig. 3*D*) exhibited increased resistance to BRAFi compared to the control (siScr) (Fig. 3 *E* and *F*). Remarkably, while BRAFi effectively inhibited extracellular signal-regulated kinase (ERK) phosphorylation (pERK1/2-T202/Y204), AMBRA1 modulation did not influence phosphorylated ERK levels in either vehicle- or BRAFi-treated cells (Fig. 3 *A* and *D*), indicating that ERK is not involved in this signal transduction mechanism. Further experiments in $BRAF^{V600E}$-mutated SK-Mel-5 cells, silenced for AMBRA1

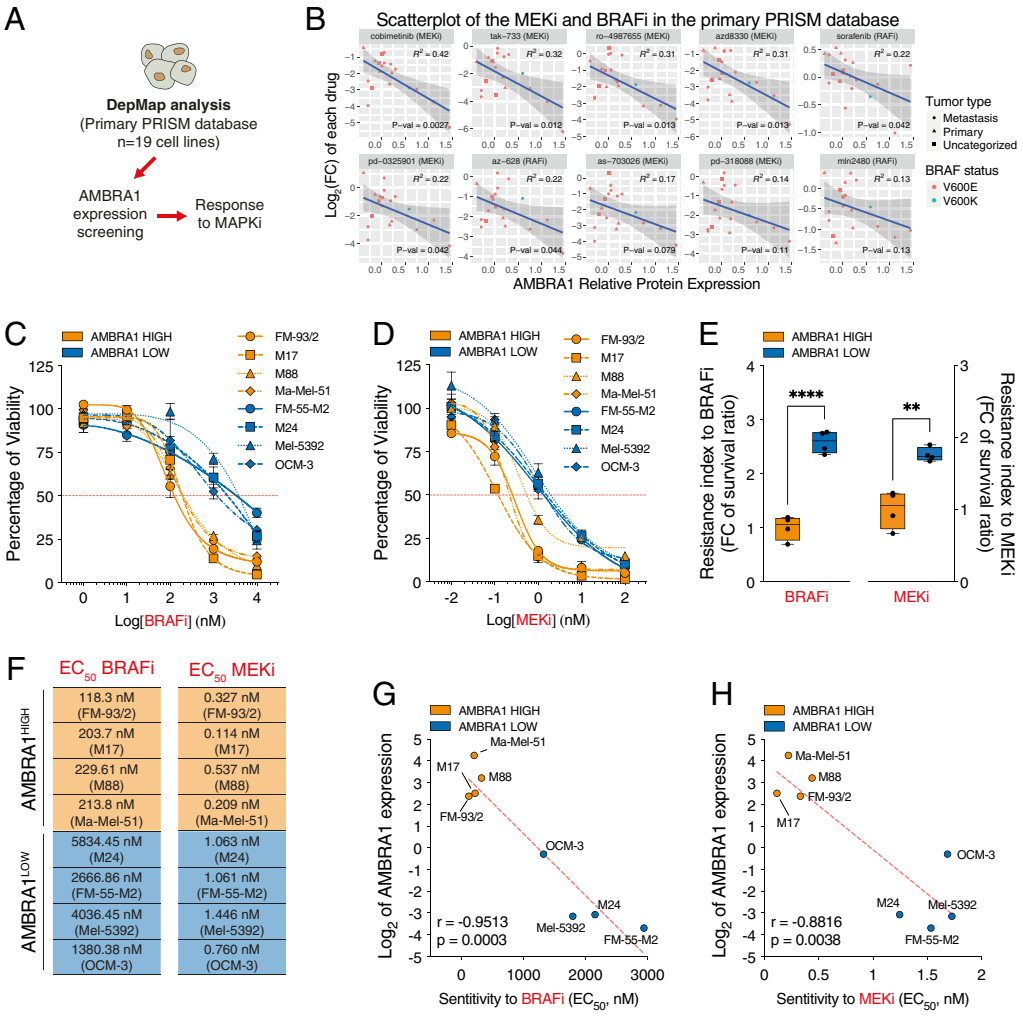

Fig. 2. Correlation between AMBRA1 and response to MAPKi. (*A*) BRAF-mutated cells from the Primary PRISM database (n = 19) were ranked for AMBRA1 expression and MAPKi response. (*B*) Scatter plots of the linear models fitted between 10 top MEKi and BRAFi median scores and AMBRA1 protein levels for the PRISM database cell lines. (*C*) Viability of $AMBRA1^{HIGH}$ (n = 4) and $AMBRA1^{LOW}$ (n = 4) cell lines after treatment with BRAFi (vemurafenib: 0.001-0.01-0.1-1-10 μM) and (*D*) MEKi (trametinib: 0.01-0.1-1-10-100 nM) for 96 h. Data are expressed as percentage vs. control cells ±SEM (n = 3 for each cell line). (*E*) Resistant index to BRAFi (vemurafenib) and MEKi (trametinib) in $AMBRA1^{HIGH}$ (n = 4) and $AMBRA1^{LOW}$ cells (n = 4) was calculated as fold change (FC) vs. the median viability values of $AMBRA1^{HIGH}$ cells ±SEM. Each dot represents a cell line (Unpaired *t* test; ****P < 0.0001; **P = 0.0017). (*F*) EC_{50} values for BRAFi (vemurafenib) and MEKi (trametinib) were derived in $AMBRA1^{HIGH}$ (n = 4) and $AMBRA1^{LOW}$ cells (n = 4) from the viability assays in (*C* and *D*). (*G*) Correlative analyses between AMBRA1 expression (Log_2) and sensitivity to BRAFi (vemurafenib; two-tailed Pearson correlation) and (*H*) the MEKi (trametinib; two-tailed Pearson correlation) in $AMBRA1^{HIGH}$ (n = 4) and $AMBRA1^{LOW}$ cells (n = 4).

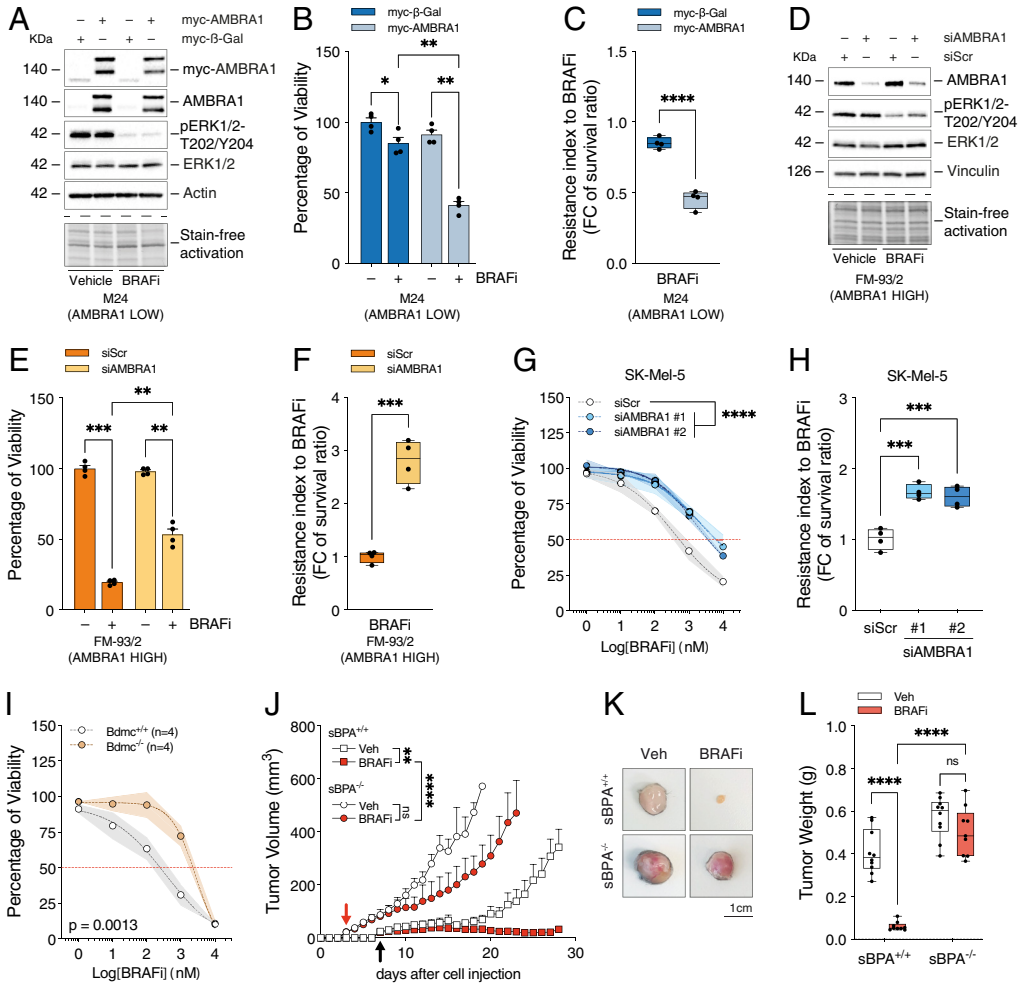

Fig. 3. Modulation of AMBRA1 links to MAPKi response. (*A*) AMBRA1^{LOW} M24 cells were transfected with a myc-AMBRA1 or a control (myc-β-Gal) plasmid and treated with BRAFi (vemurafenib, 250 nM for 96 h). Representative (n = 3) western blot of AMBRA1 (also detected with anti-myc antibody), pERK1/2-T202/Y204 and ERK1/2, Actin and stain-free activation as loading controls. (*B*) Percentage of cell viability vs. control case ±SEM (n = 4; 2-way ANOVA; **P* = 0.0119; BRAFi:myc-β-Gal vs. BRAFi:myc-AMBRA1 ***P* = 0.0071; Vehicle:myc-AMBRA1 vs. BRAFi:myc-AMBRA1 ***P* = 0.0035) and (*C*) resistant index to vemurafenib ±SEM (n = 4; Unpaired *t* test; *****P* < 0.0001). (*D*) Representative (n = 3) western blot of AMBRA1, pERK1/2-T202/Y204, ERK1/2, Vinculin and stain-free activation, (*E*) percentage of viability ±SEM (n = 4; 2-way ANOVA) and (*F*) resistant index ± SEM (n = 4; Unpaired *t* test) to vemurafenib in AMBRA1^{HIGH} FM-93/2 cells silenced for AMBRA1 (siAMBRA1) vs. control (siScr) and treated with vemurafenib 250 nM for 96 h. (*G*) Percentage of cell viability vs. control cells ± SEM (shaded areas) (n = 4; 2-way ANOVA; *****P* < 0.0001) and (*H*) vemurafenib resistance index ± SEM at 1 μM (n = 4; one-way ANOVA; siScr vs. siAMBRA1 #1 ****P* = 0.0002; siScr vs. siAMBRA1 #2 ****P* = 0.0005) in SK-Mel-5 cells silenced for AMBRA1 with two siRNAs (siAMBRA1 #1 and #2) or a control (siScr) and treated with increasing doses of vemurafenib (0.001-0.01-0.1-1-10 μM) for 72 h. (*I*) Percentage of viability of primary Bdmc wild-type (Bdmc$^{+/+}$) or knock-out (Bdmc$^{-/-}$) for *Ambra1* treated with 0.001-0.01-0.1-1-10 μM BRAFi (dabrafenib) for 96 h. Data are expressed as percentage vs. untreated cells ±SEM (shaded areas) (n = 4; sigmoidal dose–response). (*J*) Tumor growth kinetics in Vehicle (Veh)- (n = 10) or BRAFi (dabrafenib 30 mg/kg/d)- (n = 9) treated syngeneic BPA-derived (sBPA) wild-type (sBPA$^{+/+}$) and knock-out (sBPA$^{-/-}$) mice. Red and black arrows respectively indicate starting day for treatment of sBPA$^{-/-}$ and sBPA$^{+/+}$ mice. Data points represent average volume ± SD (2-way ANOVA; ***P* = 0.0065; *****P* < 0.0001). (*K*) At the time of collection, representative tumor pictures and (*L*) weights were taken (each dot represents a mouse ± SD; *****P* < 0.0001) (2-way ANOVA). ns = not significant.

using an additional siRNA (siAMBRA1 #2), revealed an elevated resistance index for both BRAFi and MEKi treatments (Fig. 3 *G* and *H* and *SI Appendix*, Fig. S3 *C* and *D*).

To validate our findings ex vivo, we employed Ambra1 wild-type [BPA-derived melanoma cell (Bdmc$^{+/+}$)] or knock-out (Bdmc$^{-/-}$) primary murine melanoma cells (*SI Appendix*, Fig. S3 *E* and *F*). This analysis confirmed a higher resistance of Bdmc$^{-/-}$ cells to both BRAFi (Fig. 3*I*) and MEKi (*SI Appendix*, Fig. S3*G*). In vivo validation involved subcutaneously injecting C57Bl/6 mice with either Bdmc$^{+/+}$ (sBPA$^{+/+}$) or Bdmc$^{-/-}$ (sBPA$^{-/-}$) cells, followed by oral treatment with BRAFi (30 mg/kg) or a control solution (Veh) for 21 d (*SI Appendix*, Fig. S3 *H* and *I*). Tumor measurements over time revealed reduced therapy response to BRAFi in sBPA$^{-/-}$ vs. sBPA$^{+/+}$ mice ($P < 0.0001$), evident in the tumor growth kinetics (Fig. 3*J*), representative images (Fig. 3*K*) and weight of tumors (Fig. 3*L*) at the time of collection.

Overall, these findings indicate that loss of AMBRA1 confers a higher resistance to MAPKi in vitro and in vivo.

Loss of AMBRA1 Correlates with a More Dedifferentiated State. A prevalent mechanism driving resistance to MAPKi in advanced melanoma is phenotype switching, a dynamic process characterized by transcriptomic features associated with invasiveness and dedifferentiation (16–19, 34–36), including expression of genes within the "Neural Crest Stem Cell-like" (NCSC-like) signature (37). Our prior transcriptomic data demonstrated an upregulation of NCSC-like-related genes in Ambra1 KO tumors (BPA$^{-/-}$) (Supplementary information in ref. 25 and *SI Appendix*, Fig. S4*A*). To further investigate this aspect, publicly available data from melanoma patients (TCGA-SKCM, n = 473) and cell lines [CCLE (Cancer Cell Line Encyclopedia), n = 49] were analyzed and samples were ranked into AMBRA1^{HIGH} and AMBRA1^{LOW} groups, based on AMBRA1 messenger RNA (mRNA) and protein expression

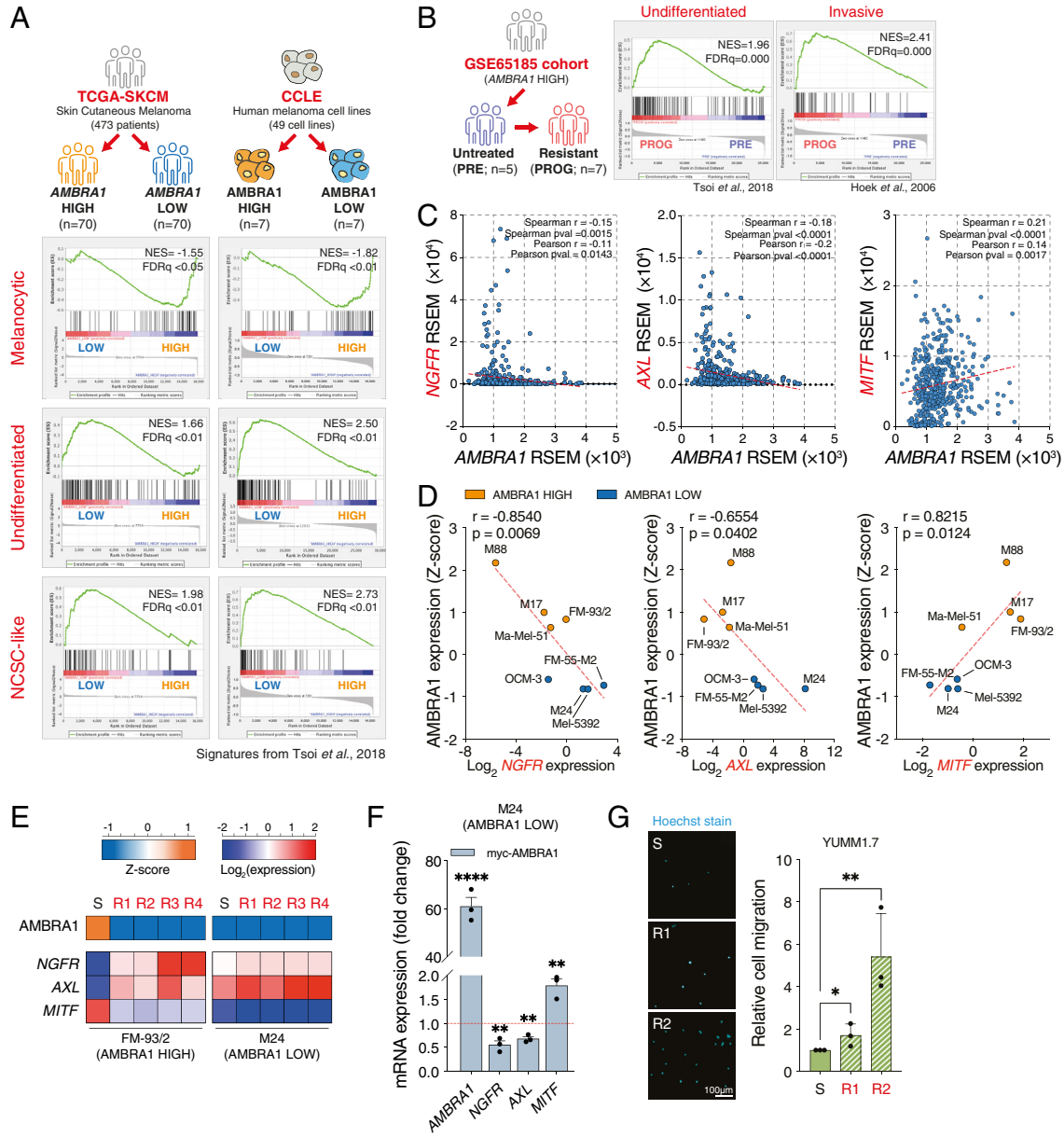

Fig. 4. AMBRA1 levels correlate with phenotype switching. (*A*) GSEA (NES = normalized enrichment score; FDR = false discovery rate) of the melanocytic, undifferentiated, and NCSC-like signatures from ref. 37 in AMBRA1^{HIGH} and AMBRA1^{LOW} groups from the TCGA-SKCM (n = 70/group) and CCLE (n = 7/group) databases and (*B*) of the Undifferentiated (37) and Invasive (38) signature in the untreated (PRE) vs. resistant (PROG) tumors of the AMBRA1^{HIGH} group of the GSE65185 cohort (n = 5 to 7/group). (*C*) Pearson correlation analyses between AMBRA1 expression and Log_2 expression of *NGFR*, *AXL*, and *MITF* in the TCGA-SKCM datasets (n = 443) and (*D*) in the human AMBRA1^{HIGH} (FM-93/2, M17, M88, Ma-Mel-51) and AMBRA1^{LOW} (FM-55/M2, M24, Mel-5392, OCM-3) cell lines (after normalization on internal control *L34*). (*E*) RT-qPCR (n = 3) of *NGFR*, *AXL*, and *MITF* in the vemurafenib-resistant FM-93/2- and M24-derived R1-R4 cell lines vs. sensitive (S) lines. Data are expressed as fold change ±SEM (n = 3; 2-way ANOVA). The heatmap of the expression levels of AMBRA1 was derived from densitometry in Fig. 1*E*. (*F*) RT-qPCR data ±SEM of AMBRA1^{LOW} M24 cells transfected for 48 h with a myc-AMBRA1-encoding plasmid vs. control cells (myc-β-Gal, red line) (n = 3; Unpaired *t* test; *AMBRA1*: ****$P < 0.0001$; *NGFR*: **$P = 0.0054$; *AXL*: **$P = 0.002$; *MITF*: **$P = 0.0049$). (*G*) Representative pictures and quantification of relative cell migration ±SD of YUMM1.7-derived R1 and R2 vemurafenib-resistant cells toward sensitive (S) cells (n = 3; Unpaired *t* test; *$P = 0.0423$; **$P = 0.0099$).

levels, respectively (Fig. 4*A*). Gene Set Enrichment Analysis (GSEA) indicated a significant enrichment for "Undifferentiated" and NCSC-like gene sets (37) in the AMBRA1^{LOW} groups, while the "Melanocytic" gene set (37) was enriched in the AMBRA1^{HIGH} groups (Fig. 4*A*). These results indicate that AMBRA1^{LOW} tumors exhibit genetic features of dedifferentiation. A significant enrichment for the Undifferentiated signature was observed in the AMBRA1^{LOW} MAPKi-resistant tumors (PROG) derived from the AMBRA1^{HIGH} pretreatment group (PRE) in both the GSE65185 (Fig. 4*B*) and GSE50509 cohorts (*SI Appendix*, Fig. S4*B*) as well as in posttreatment samples from the GSE129127 PDX platform (*SI Appendix*, Fig. S4*C*).

We further characterized this aspect by selecting key regulator genes for these signatures, namely *NGFR* and *AXL* (for the Undifferentiated and NCSC-like signatures), and *MITF* (for the Melanocytic state). *NGFR* and *AXL* expression negatively correlated, whereas *MITF* expression positively correlated with AMBRA1 at mRNA or protein level, respectively, in both the TGCA-SKCM dataset (n = 443) (Fig. 4*C*) and in the AMBRA1^{HIGH}/AMBRA1^{LOW} melanoma cell panel (Fig. 4*D*).

To investigate the link between AMBRA1-dependent resistance to BRAFi and phenotype switching, we analyzed the expression of *NGFR*/*AXL*/*MITF* upon acquired resistance in AMBRA1^{HIGH} FM-93/2 cells. Remarkably, chronic exposure of AMBRA1^{HIGH}

FM-93/2 cell line to BRAFi induced a switch from an $NGFR^{LOW}/AXL^{LOW}/MITF^{HIGH}$ profile (characterizing sensitive cells) to an $NGFR^{HIGH}/AXL^{HIGH}/MITF^{LOW}$ profile (which instead typifies R1-R4 BRAFi-resistant cells) (Fig. 4*E* and *SI Appendix*, Fig. S4 *D–F*). By contrast, $AMBRA1^{LOW}$ M24 resistant cells show similar genetic features of the sensitive counterpart (Fig. 4*E* and *SI Appendix*, Fig. S4 *D–F*). These results reinforce the notion that $AMBRA1^{LOW}$ cells possess a dedifferentiated genetic state. As a matter of fact, $AMBRA1^{LOW}$ M24 cell line reconstitution with AMBRA1 (myc-AMBRA1) led to a significant reversal of gene expression toward a more differentiated state ($NGFR^{LOW}/AXL^{LOW}/MITF^{HIGH}$) (Fig. 4*F*), which was accompanied by restored sensitivity to BRAFi (Fig. 3 *A–C*). Consistent with previous data showing increased metastatic potential of melanoma cells upon AMBRA1 deficiency (25), GSEAs also established an association between $AMBRA1^{LOW}$ MAPKi-resistant tumors and an enriched invasive signature (38) in all cohorts analyzed (Fig. 4*B* and *SI Appendix*, Fig. S4 *B* and *C*). Accordingly, BRAFi-resistant cells of both murine (Fig. 4*G*) and human (*SI Appendix*, Fig. S4*G*) origin displayed higher cell migration capacity. Reconstitution experiments with an AMBRA1-encoding plasmid reduced relative cell migration, proving a direct link between AMBRA1 and invasiveness of BRAFi-resistant cells (*SI Appendix*, Fig. S4*H*).

Altogether, these results indicate that low expression levels of AMBRA1 are indicative of a phenotype switch toward a more invasive/dedifferentiated and BRAFi-resistant state (*SI Appendix*, Fig. S4*I*).

Loss of AMBRA1 Confers Resistance to BRAFi through Focal Adhesion Kinase 1 (FAK1) Activation. The NCSC-like state has been associated with activation of the FAK1 pathway in melanoma cell subclones exhibiting resistance to MAPKi (14). Our findings reveal that $AMBRA1^{LOW}$ cells display a NCSC-like gene expression state (Fig. 4), along with resistance to MAPKi (Fig. 2). Consistent with our previous study demonstrating hyperactivated FAK1 signaling upon AMBRA1 deficiency in melanoma (25), all FM-93/2-derived BRAFi-resistant cell lines displaying features of the NCSC-like state (Fig. 4*E* and *SI Appendix*, Fig. S4 *D–F*) exhibited elevated levels of phosphorylated FAK-Y397 (pFAK-Y397), when compared to the sensitive line (Fig. 5 *A* and *B*).

To further support this evidence, we investigated FAK1 activation following acute BRAFi treatment in AMBRA1-silenced SK-Mel-5 cells (Fig. 5*C* and *SI Appendix*, Fig. S5*A*). In this setting, higher levels of pFAK-Y397 and of its downstream target pSRC-Y416 were observed (Fig. 5 *C* and *D* and *SI Appendix*, Fig. S5*B*), while AMBRA1 silencing did not affect the phosphorylation status of pERK1/2-T202/Y204 (Fig. 5*C* and *SI Appendix*, Fig. S5*C*), consistent with previous observations (Fig. 3 *A* and *D*). Similar significant results were obtained in BRAFi-treated syngeneic $sBPA^{-/-}$ vs. $sBPA^{+/+}$ mice (Fig. 5 *E* and *F* and *SI Appendix*, Fig. S5*D*).

We next aimed to establish a direct link between AMBRA1, FAK1 activation, and therapy resistance by conducting cell viability assays. Transient transfection with a plasmid encoding a mutant form of AMBRA1 ($AMBRA1^{P170S}$) (Fig. 5 *G* and *H*) mimicking the AMBRA1-deficient FAK1-related phenotype (characterized by elevated pFAK-Y397) (28, 29), significantly increased the resistance index to BRAFi in both FM-93/2 (Fig. 5 *I* and *J*) and M24 (*SI Appendix*, Fig. S5 *E–G*) cells, compared to $AMBRA1^{WT}$-expressing cells. In a similar fashion, we silenced FAK1 (siFAK1) in FM-93/2 cells and re-expressed either the WT ($FAK1^{WT}$) or the P876A/P882A mutant ($FAK1^{AA}$) form of FAK1, which abrogates the AMBRA1/FAK1 interaction mimicking the AMBRA1-deficient-like phenotype of FAK1 activation (Fig. 5*G*) (25). Analogous to results described for the $AMBRA1^{P170S}$ mutant, BRAFi-treated $FAK1^{AA}$-expressing cells (Fig. 5*K*) showcased higher resistance to BRAFi than the control (FAK^{WT}) cells (Fig. 5 *L* and *M*).

Moreover, FM-93/2-derived BRAFi-resistant cells displayed a reduction of the active form of the bona fide autophagy marker LC3 (LC3-II) compared to sensitive cells (Fig. 5*A* and *SI Appendix*, Fig. S5*H*). To evaluate the involvement of the proautophagic function of AMBRA1 (20, 21) in BRAFi resistance, we performed reconstitution experiments of a mutant form impairing AMBRA1 autophagy function ($AMBRA1^{LIRaa}$) in M24 cells followed by BRAFi treatment (*SI Appendix*, Fig. S5*I*). Our results do not support AMBRA1-mediated regulation of autophagy as an additional mechanism contributing to therapy resistance to BRAFi (*SI Appendix*, Fig. S5 *J* and *K*).

Taken together, these results indicate that AMBRA1-dependent activation of FAK1 signaling in melanoma is responsible for increased resistance to BRAFi.

Targeting FAK1 Overcomes BRAFi Resistance of $AMBRA1^{LOW}$ Melanoma. To address the therapeutic relevance of our findings, we tested the efficacy of pharmacological inhibition of FAK1, either alone or in combination with BRAFi, for melanoma treatment. To assess this, we subjected $AMBRA1^{HIGH}$ FM-93/2 and $AMBRA1^{LOW}$ M24 cells to FAKi or a combination of FAKi and BRAFi (Fig. 6*A*) and evaluated cell viability using the ratio between FAKi treatment and its corresponding control cases (*Materials and Methods*) (*SI Appendix*, Fig. S6*A*). Consistent with earlier findings (25), $AMBRA1^{LOW}$ M24 cells exhibited sensitivity to FAKi, further enhanced upon combined therapy with BRAFi (Fig. 6*B* and *SI Appendix*, Fig. S6*A*). Conversely, $AMBRA1^{HIGH}$ FM-93/2 cells demonstrated unresponsiveness to FAKi, with no additional effect induced by BRAFi cotreatment (Fig. 6*B* and *SI Appendix*, Fig. S6*A*). To validate the AMBRA1 dependence of this response, we employed propidium iodide (PI) staining followed by FACS analyses in SK-Mel-5 silenced for AMBRA1 (siAMBRA1), obtaining results in line with $AMBRA1^{LOW}$ M24 and $AMBRA1^{HIGH}$ FM-93/2 cells (*SI Appendix*, Fig. S6 *B* and *C*).

Subsequently, we extended our investigation to Ambra1 WT and KO cells ($Bdmc^{+/+}$ and $Bdmc^{-/-}$) by employing two different FAKi (PF-56227 and defactinib) (*SI Appendix*, Fig. S6 *D* and *E*). In either case, the combined treatment with BRAFi elicited only a marginal additional response in $Bdmc^{-/-}$ cells compared to FAKi treatment alone, mirroring the response of $Bdmc^{+/+}$ cells to BRAFi (Fig. 6*C* and *SI Appendix*, Fig. S6*F*). Similar outcomes were obtained in a syngeneic model of mice orally administered a combined BRAFi (30 mg/kg) and FAKi (50 mg/kg) therapy (*SI Appendix*, Fig. S6 *G* and *H*).

Subsequent testing of FAKi efficacy in $AMBRA1^{LOW}$ FM-93/2- (Fig. 6*D*), M17- (*SI Appendix*, Fig. S6*I*), YUMM1.7- (*SI Appendix*, Fig. S6*J*), and YUMM1.1- (*SI Appendix*, Fig. S6*K*) derived BRAFi-resistant cells demonstrated a significantly increased response to FAKi treatment compared to respective controls, unlike the $AMBRA1^{HIGH}$ sensitive cell line.

Altogether, these results underscore the potential of FAKi utilization to overcome melanoma resistance to BRAFi in tumors exhibiting low AMBRA1 expression.

Cellular Heterogeneity in AMBRA1 Expression Is a Determinant of BRAFi Resistance Development. Given the strong correlation between AMBRA1 expression and response to BRAFi in both clinical and experimental contexts, we speculated whether the propensity of some melanomas to develop BRAFi resistance could be attributed to intratumor heterogeneity of AMBRA1 expression. Indeed, from a first analysis by immunofluorescence, we identified a small cell population exhibiting lower AMBRA1 signal in the $AMBRA1^{HIGH}$ FM-93/2 cells (*SI Appendix*, Fig. S7*A*). To further investigate this,

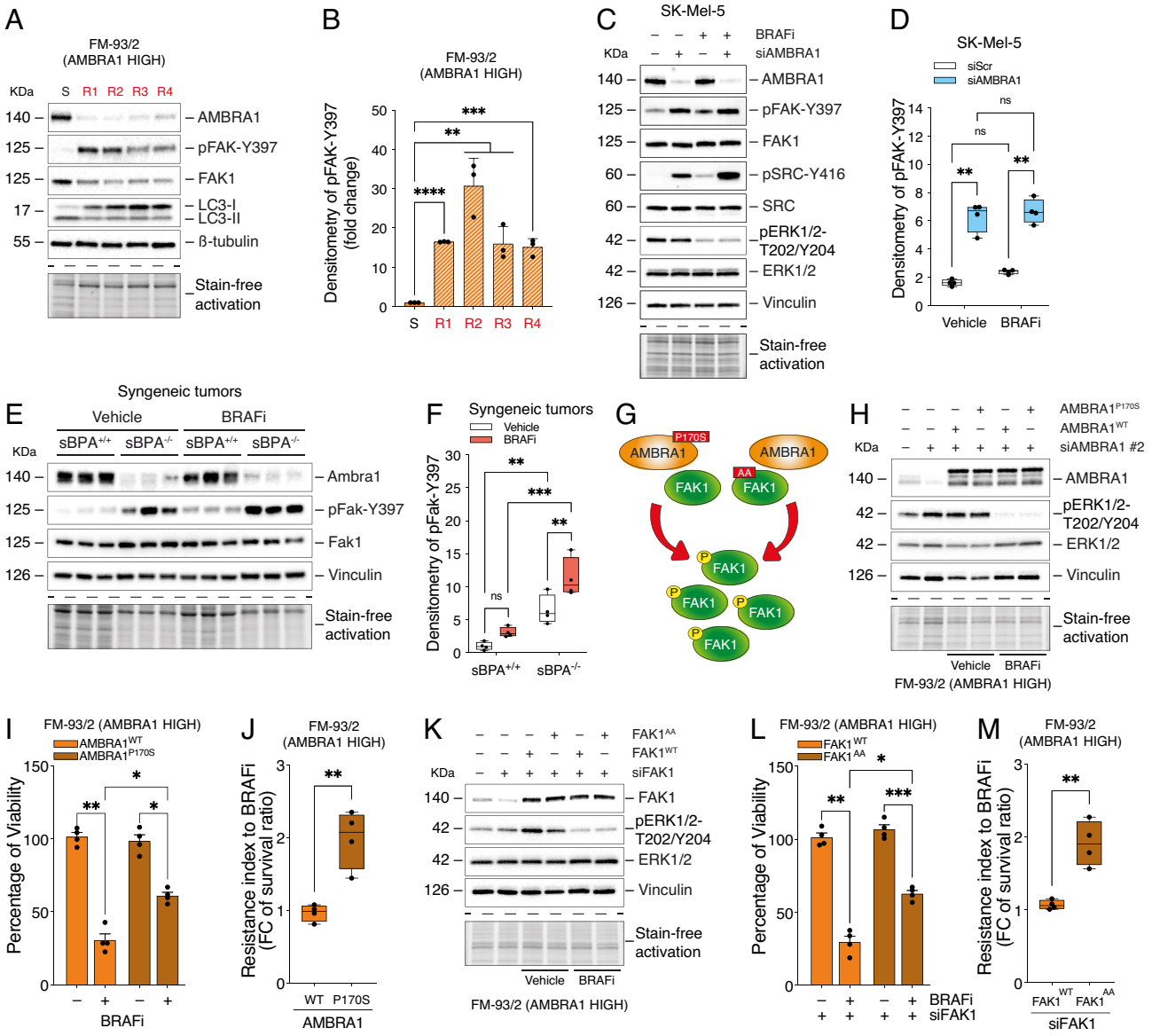

Fig. 5. AMBRA1-related MAPKi resistance relies on FAK1 activation. (*A*) Representative western blot (n = 3) of AMBRA1, pFAK-Y397, and FAK1, LC3 (LC3-I and LC3-II) and of β-tubulin and stain-free activation (loading controls) in FM-93/2-derived vemurafenib-resistant cell lines (R1 to R4) vs. sensitive (S) and (*B*) densitometry of pFAK-Y397 after normalization on FAK1 and β-tubulin (n = 3; ±SD; Unpaired *t* test; R1 vs. S ****$P < 0.0001$, R2 vs. S **$P = 0.0018$, R3 vs. S **$P = 0.004$, R4 vs. S ***$P = 0.0004$). (*C*) Representative (n = 4) western blot of FAK1 signaling markers, ERK1/2 and phosphorylated form (T202/Y204) in SK-Mel-5 cells silenced for AMBRA1 (siAMBRA1 #1) vs. control (siScr) and treated with 10 μM vemurafenib for 72 h. Vinculin and stain-free activation: loading, AMBRA1: transfection controls. (*D*) pFAK-Y397 densitometry of *C* (n = 4; ±SD; 2-way ANOVA; Vehicle:siScr vs. Vehicle:siAMBRA1 **$P = 0.001$; BRAFi:siScr vs. BRAFi:siAMBRA1 **$P = 0.0013$). (*E*) Representative western blot (n = 3/group) of Ambra1, pFak-Y397, and Fak1 in BRAFi (dabrafenib)- vs. Vehicle-treated $sBPA^{-/-}$ and $sBPA^{+/+}$ tumors, and (*F*) pFak-Y397 densitometry (n = 4; 2-way ANOVA; Vehicle:$sBPA^{+/+}$ vs. Vehicle:$sBPA^{-/-}$ **$P = 0.0053$; Vehicle:$sBPA^{-/-}$ vs. BRAFi:$sBPA^{-/-}$ **$P = 0.0077$; ***$P = 0.0006$). (*G*) Schematic function of the $AMBRA1^{P170S}$ and $FAK1^{AA}$ mutants on FAK1 signaling (high pFAK-Y397 levels). (*H*) FM-93/2 cells silenced for endogenous AMBRA1 (siAMBRA1 #2) were transfected with myc-$AMBRA1^{WT}$ or ^{P170} plasmids and treated with BRAFi (vemurafenib: 250 nM, 72 h). Western blot (n = 3) for AMBRA1: transfection, pERK1/2-T202/Y204 and ERK1/2: treatment, Vinculin and stain-free activation: loading controls. (*I*) Cell viability (±SEM) (n = 4; 2-way ANOVA; Vehicle:$AMBRA1^{P170S}$ vs. BRAFi:$AMBRA1^{P170S}$ *$P = 0.0223$; BRAFi:$AMBRA1^{WT}$ vs. BRAFi:$AMBRA1^{P170S}$ *$P = 0.0207$; **$P = 0.0051$) and (*J*) resistance index to vemurafenib (n = 4; Unpaired *t* test; **$P = 0.0026$) were measured. (*K*) FM-93/2 cells were silenced for endogenous FAK1 (siFAK1), transfected with either $FAK1^{WT}$ or ^{AA} plasmids and treated as in (*H*). Western blot (n = 3) for FAK1: transfection, pERK1/2-T202/Y204 and ERK1/2: treatment, Vinculin and stain-free activation: loading controls. (*L*) Both the cell viability ±SEM (n = 4; 2-way ANOVA; *$P = 0.013$; **$P = 0.009$; ***$P = 0.0004$) and (*M*) the resistance index ±SEM to vemurafenib (n = 4; Unpaired *t* test; **$P = 0.0017$) for cells transfected and treated as in *K* were measured. ns=not significant.

we generated single-cell-derived subclones from the human FM-93/2 and the murine YUMM1.7 cell lines, which both express high levels of AMBRA1, and performed a retrospective analysis of AMBRA1 expression in these subclones following exposure to BRAFi. The initial assessment unveiled a highly variable response to BRAFi among the subclones of both cell lines (Fig. 6 *E* and *F*). Subsequently, we identified the top BRAFi-sensitive and -resistant subclones based on a 20% (FM-93/2) or 15% (YUMM1.7) cut-off on the BRAFi resistance index. RT-qPCR and western blot analyses revealed that subclones with the highest BRAFi resistance index exhibited genetic features of phenotype switching (*SI Appendix*, Fig. S7 *B* and *C*) and reduced AMBRA1 levels in both the FM-93/2 (clone 1.D12; 19% response to BRAFi; Fig. 6*G*) and YUMM1.7 (clones 2.B10, 1.D7, and 2.G5; 19%, 10%, and 9.5% response to BRAFi, respectively; Fig. 6*H*) models. This supports the hypothesis of a subclonal heterogeneous AMBRA1 expression in melanoma prior to treatment.

Furthermore, elevated levels of pFAK-Y397 were detected in the top therapy-resistant subclones (Fig. 6 *G* and *H*), showing a strong inverse correlation with AMBRA1 expression levels in FM-93/2

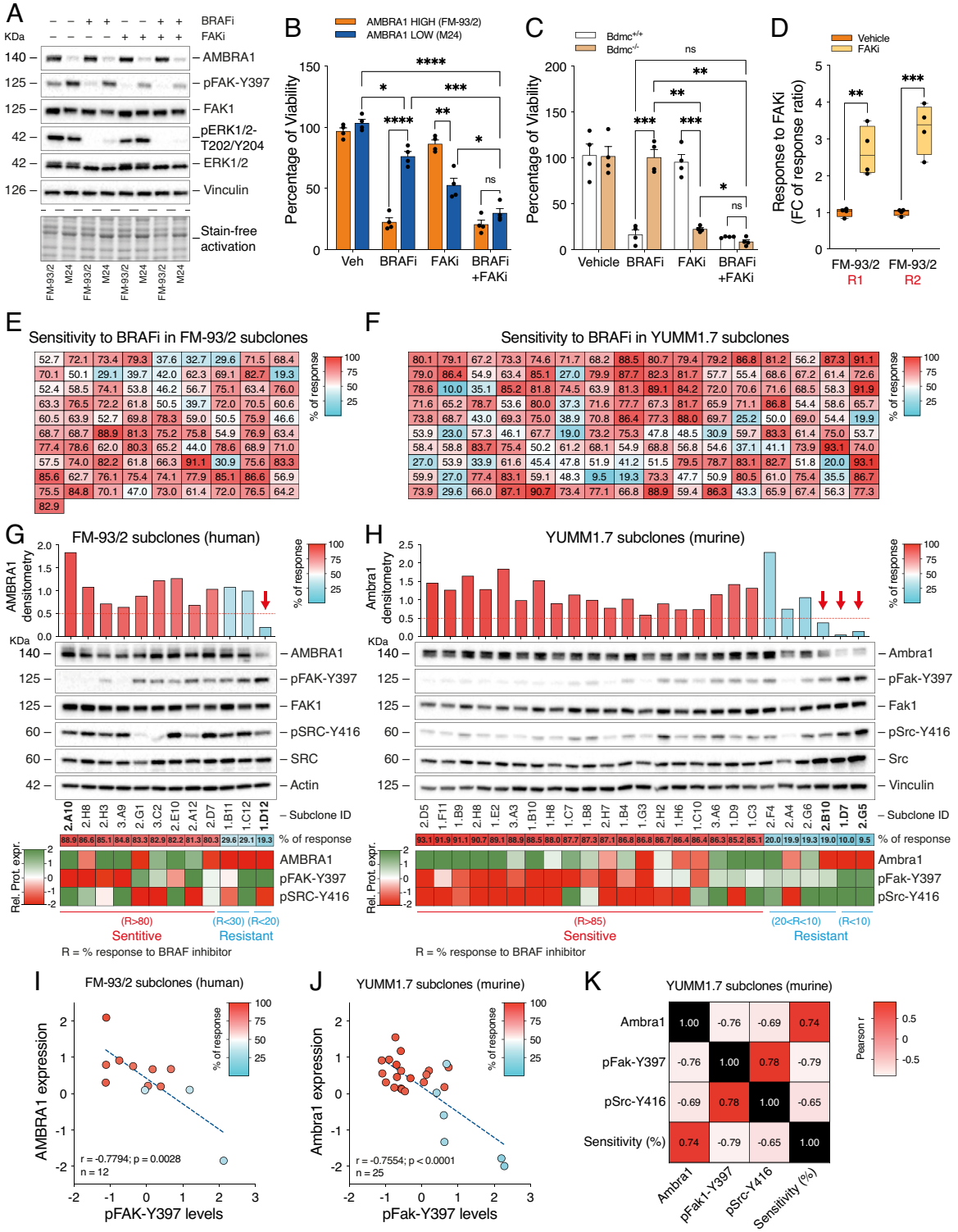

Fig. 6. AMBRA1 expression heterogeneity and BRAFi resistance development. (*A*) Western blot (n = 3) of FM-93/2 and M24 cells treated with BRAFi (vemurafenib, 250 nM) and/or FAKi (defactinib, 5 μM) for 96 h; pFAK-Y397 and pERK1/2-T202/Y204: treatment, actin, and stain-free activation: loading controls. (*B*) Percentage of viability ±SEM (vs. control) of cells in *A* (n = 4; 2-way ANOVA; Veh:AMBRA1 LOW (M24) vs. BRAFi:AMBRA1 LOW (M24) **P* = 0.0101; FAKi:AMBRA1 LOW (M24) vs. BRAFi+FAKi:AMBRA1 LOW (M24) **P* = 0.0333; ***P* = 0.0020; ****P* = 0.0002; *****P* < 0.0001). (*C*) Percentage of cell viability ±SEM of $Bdmc^{+/+}$ and $Bdmc^{-/-}$ cells treated with BRAFi (dabrafenib, 500 nM) and/or FAKi (PF-562271, 5 μM) for 96 h (n = 4/group; **P* = 0.0335; $Bdmc^{-/-}$:BRAFi vs. $Bdmc^{-/-}$:FAKi ***P* = 0.0082; $Bdmc^{-/-}$:BRAFi vs. $Bdmc^{-/-}$:BRAFi+FAKi ***P* = 0.0082; $Bdmc^{+/+}$:BRAFi vs. $Bdmc^{-/-}$:BRAFi ****P* = 0.0001; $Bdmc^{+/+}$:FAKi vs. $Bdmc^{-/-}$:FAKi ****P* = 0.0005). (*D*) Response to FAKi ±SEM (vs. control) in FM-93/2-derived R1 and R2 cells treated with defactinib 5 μM for 72 h (n = 4; Unpaired *t* test). (*E*) Sensitivity to BRAFi in single-cell-derived FM-93/2 (vemurafenib; n = 91) and (*F*) YUMM1.7 (dabrafenib; n = 160) subclones after treatment with a 250 nM dose for 96 h. Each square represents a subclone and the enclosed values the percentage of response vs. untreated cells (n = 3). (*G*) Representative western blot analysis (n = 3) of AMBRA1, pFAK-Y397, FAK1, pSRC-Y416, and SRC in the top sensitive and resistant single-cell-derived FM-93/2 (n = 12) and (*H*) YUMM1.7 (n = 25) subclones. Densitometry of AMBRA1 is shown as ratio on Actin/Vinculin and as heatmap. The red line in the graphs denotes applied cut-off, while the red arrow the subclone with AMBRA1/Ambra1 expression below cut-off (≤0.5). Densitometry of pFAK-Y397 and pSRC-Y416 are shown as heatmap after normalization on FAK1 and SRC, respectively, and the loading control. (*I* and *J*) Values of densitometry from the heatmaps in *G* and *H* have been used for the correlative analyses between AMBRA1 and pFAK1-Y397 expression in both (*I*) FM-93/2- (n = 12; two-tailed Pearson correlation) and (*J*) YUMM1.7- (n = 25; two-tailed Pearson correlation) derived subclones. (*K*) Pearson r coefficient for the interrelation between Ambra1, pFak-Y397, and pSrc-Y416 and sensitivity to dabrafenib in YUMM1.7-derived subclones (n = 25). ns = not significant.

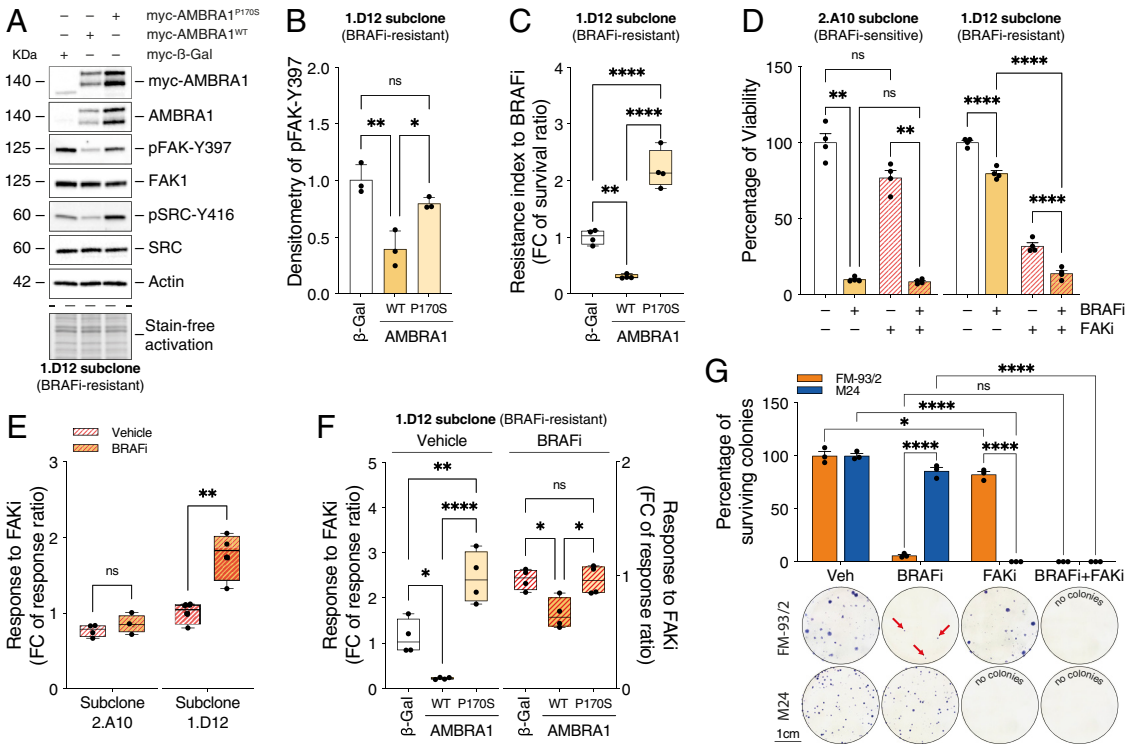

Fig. 7. Analysis of AMBRA1^{LOW} subclones in response to BRAFi and FAKi. (*A*) FM-93/2-derived 1.D12 subclone was transfected with myc-AMBRA1^{WT} or myc-AMBRA1^{P170} and with the control plasmid myc-β-Gal. Western blot analyses for the FAK1 signaling markers were performed (n = 3). AMBRA1 was also detected with an anti-myc antibody. Actin and stain-free activation were used as loading controls. (*B*) Densitometry analysis of pFAK-Y397 in *A* after normalization on total FAK1 and Actin (n = 3; ±SD vs. β-Gal; one-way ANOVA; *P = 0.0226; **P = 0.0029). (*C*) Resistance index to BRAFi for cells in *A* after treatment with 250 nM vemurafenib for 72 h (n = 4; ±SD vs. β-Gal; one-way ANOVA; **P = 0.0032; ****P < 0.0001). (*D*) Percentage of cell viability ±SEM of FM-93/2-derived 2.A10 and 1.D12 subclones after 96 h of treatment with FAKi (defactinib, 2.5 μM) and/or BRAFi (vemurafenib, 250 nM) (n = 4; Unpaired *t* test; 2.A12 Vehicle:BRAFi **P = 0.001; 2.A12 BRAFi:BRAFi+FAKi **P = 0.0023; ****P < 0.0001) and (*E*) response to FAKi alone (Vehicle) or in combination with vemurafenib (BRAFi) (n = 4; ±SEM; Unpaired *t* test; **P = 0.0053). (*F*) Response to FAKi ±SEM (defactinib, 2.5 μM) alone (Vehicle) (n = 4; one-way ANOVA) or in combination with BRAFi (vemurafenib, 250 nM) (BRAFi) (n = 4; one-way ANOVA; Vehicle β-Gal vs. AMBRA1^{WT} *P = 0.0291; BRAFi β-Gal vs. AMBRA1^{WT} *P = 0.0182; BRAFi AMBRA1^{WT} vs. AMBRA1^{P170S} *P = 0.02; **P = 0.0034; ****P < 0.0001) in 1.D12 cells transfected with myc-AMBRA1^{WT} or myc-AMBRA1^{P170} and with the control plasmid myc-β-Gal. (*G*) Representative pictures of colony formation assay and percentage of surviving colonies ±SD (vs. control) of FM-93/2 and M24 cells treated for 21 d with BRAFi (vemurafenib, 250 nM) and/or FAKi (defactinib, 500 nM) (n = 3; 2-way ANOVA; *P = 0.0151; ****P < 0.0001). ns = not significant.

(r = −0.7794; P = 0.0028; Fig. 6*I*) and YUMM1.7 (r = −0.5137; P = 0.0086; Fig. 6*J*) subclones. Phosphorylation of Src (pSrc-Y416) was also detected in the least BRAFi-sensitive YUMM1.7-derived subclones (Fig. 6*H* and *SI Appendix*, Fig. S7*D*), confirming full activation of the FAK1 signaling pathway. Pearson's correlation analysis confirmed the interdependency among response to BRAFi, Ambra1 expression, and pFak-Y397 and pSrc-Y416 levels (Fig. 6*K*).

To establish a direct link between AMBRA1 expression and FAK1 activation in the top BRAFi-resistant subclones, we reconstituted the FM-93/2 AMBRA1^{LOW}/pFAK-Y397^{HIGH} 1.D12 subclone with either WT AMBRA1 (myc-AMBRA1^{WT}) or the single-point mutant P170S (myc-AMBRA1^{P170S}) (Fig. 7*A*). Expression of AMBRA1^{WT} induced a complete rescue of FAK1 signaling, whereas the AMBRA1^{P170S}-expressing cells exhibited phospho-activation levels of FAK1 and SRC similar to control cells (Fig. 7 *A* and *B* and *SI Appendix*, Fig. S7*E*), indicating AMBRA1-dependent activation of FAK1 signaling in BRAFi-resistant subclones. Moreover, analysis of cell viability showed that ectopic expression of AMBRA1^{P170S} restored cellular resistance to BRAFi (Fig. 7*C* and *SI Appendix*, Fig. S7*F*).

Consistent with these results, the FM-93/2-derived AMBRA1^{LOW}/pFAK-Y397^{HIGH} 1.D12 subclone (*SI Appendix*, Fig. S7*G*) displayed high sensitivity to FAKi alone, which was further enhanced in cotreatment with BRAFi (Fig. 7 *D* and *E*). Conversely, the AMBRA1^{HIGH}/pFAK-Y397^{LOW} 2.A10 subclone (*SI Appendix*, Fig. S7*G*) exhibited limited response to FAK1 inhibition, whether used as a single treatment or in combination with BRAFi (Fig. 7 *D* and *E*). Cells from the 1.D12 subclone re-expressing AMBRA1^{WT} also corroborated the AMBRA1 dependence of such response (Fig. 7*F*), whereas AMBRA1^{P170S}-expressing cells exhibited either a higher response to FAKi or a response to combined therapy comparable to control cells (β-Gal) (Fig. 7*F*).

These findings strongly suggest that the expression levels of AMBRA1 in the tumor are potentially predictive of whether treatment with FAKi should be administered as mono- or combined therapy to overcome BRAFi resistance in melanoma. To validate this hypothesis, we performed colony formation assays in AMBRA1^{LOW} M24 and AMBRA1^{HIGH} FM-93/2 cells upon FAKi treatment as monotherapy or in combination with BRAFi. FAKi monotherapy effectively prevented colony formation in AMBRA1^{LOW} M24 cells, with combined therapy with BRAFi showing no additional effects (Fig. 7*G*). Conversely, FAKi monotherapy exerted only limited effects on colony formation in the AMBRA1^{HIGH} FM-93/2 cells (Fig. 7*G*). In this cell line, resistant colonies to BRAFi eventually emerged upon prolonged treatment with BRAFi, which ability to grow was overcome upon combined treatment with FAKi (Fig. 7*G*).

Overall, these data strongly suggest that AMBRA1 expression levels in the tumor serve as a predictor for FAKi mono- or BRAFi-combined therapy to overcome therapy resistance in melanoma.

Discussion

MAPKi therapy has emerged as a pivotal treatment strategy for advanced metastatic melanoma (8, 11–13), driven by the identification of activating *BRAF* missense mutations in a high percentage of patients (39). Despite the current widened landscape of newly

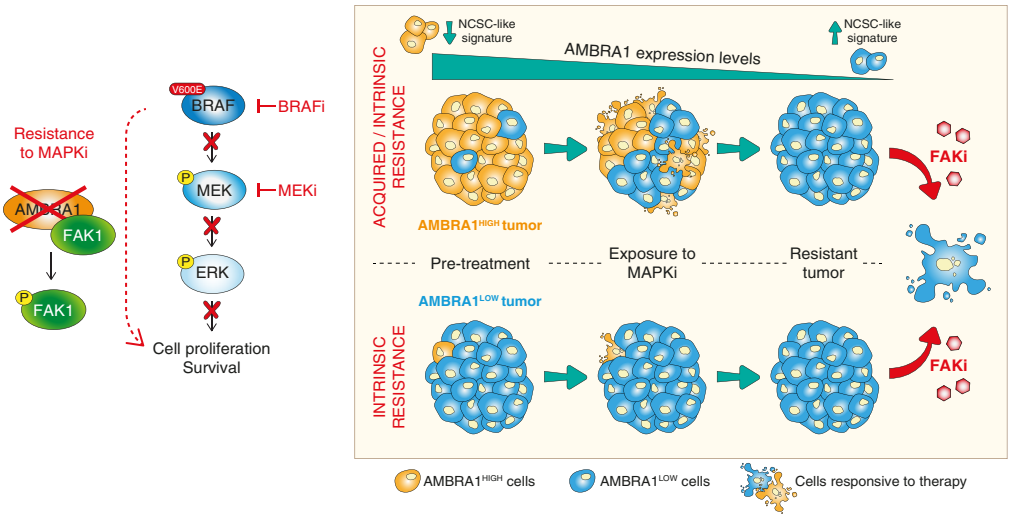

Fig. 8. AMBRA1 levels predict melanoma resistance to targeted therapy. Loss or reduced expression of AMBRA1 leads to increased resistance of melanoma to MAPKi treatment (BRAFi and MEKi) by means of a MAPK-independent pathway. This involves the hyperactivation (phosphorylation) of the FAK1 (*Left*). AMBRA1^{HIGH} tumors show low expression of AMBRA1 after prolonged exposure to BRAFi, together with increased expression of NCSC-like genes. AMBRA1^{LOW} tumors show features of intrinsic resistance to MAPKi, including high expression for NCSC-like genes. Targeting FAK1 with FAK inhibitors (FAKi) overcomes MAPKi resistance in AMBRA1^{LOW} tumors and prevents the establishment of resistance in AMBRA1^{HIGH} tumors (*Right*).

developed and clinically approved MAPKi drugs and the associated clinical achievements (4, 6, 7, 9, 10), the occurrence of resistance, whether intrinsic or acquired, remains a significant challenge in late-stage melanoma treatment (12, 13). While MAPK-dependent mechanisms typically involve the reactivation of the MAPK pathway to counteract BRAF^{V600E} inhibition (30, 40), our study provides evidence for a MAPK (ERK1/2)-independent mechanism of MAPKi resistance, specifically mediated by the AMBRA1-dependent activation of FAK1 signaling pathway.

In 2015, the random insertion of transposons into the genome of melanoma-bearing mice (*Sleeping Beauty* transposon mutagenesis) identified *Ambra1* among novel candidates, alongside well-known genes (e.g., *Braf, Cdkn2a, Pten,* and *Mitf*), contributing to melanoma progression and BRAFi resistance (supplementary material in ref. 41). After highlighting the tumor suppressor function of *Ambra1* in melanoma (25), our results now show that pretreatment melanomas with naturally low levels of AMBRA1, AMBRA1^{LOW} subclones derived from AMBRA1-proficient melanoma cells, and mice bearing Ambra1 KO melanoma, all exhibit increased resistance to MAPKi treatment. Our present research places AMBRA1 as a determinant of melanoma response to MAPKi, hence expanding our previous understanding of AMBRA1 as a regulator of growth and metastatic potential in melanoma, related to findings obtained in preclinical mouse models and cell-based systems (25).

Furthermore, this study consolidates previous genetic evidence of Ambra1 KO tumors (25), substantiating the presence of features associated with invasiveness and dedifferentiation (NCSC-like) in AMBRA1^{LOW} TCGA-SKCM samples and cell lines. This dedifferentiated state not only denotes more aggressive and invasive tumors (24, 25), but also outlines the presence of a driving genetic program for MAPKi resistance, termed "phenotype switching" (16–19, 34–36) in melanomas with low AMBRA1 expression. Consistently, restoring AMBRA1 expression in AMBRA1^{LOW} cells reverses their dedifferentiated and migrating state, reinforcing the hypothesis that loss of AMBRA1 favors phenotype switching in melanoma.

FAK1 activation has previously been associated with MAPKi resistance of melanoma both in a non-cell-autonomous and cell-autonomous context (14, 42). MAPK inhibition was shown to induce extracellular matrix remodeling by tumor-associated fibroblasts, with consequent integrin/FAK1 signaling activation (42). Additionally, MAPK inhibition can also activate FAK1 signaling in NCSC melanoma cells derived from drug-resistant PDX tumors in a cell-autonomous manner (14). Sensitivity to FAK1 inhibition is increased in these tumors (33), in which we detected low expression levels of AMBRA1. In our study, we show that AMBRA1^{LOW} cells and subclones display resistance to MAPKi coupled with FAK1 signaling hyperactivation and sensitization to FAK1 inhibitors (FAKi).

Comprehensively, our findings shed further light not only on the multifaceted biological nature of AMBRA1 and its functional relationship with FAK1, but also on the clinical implications of this interplay. First, AMBRA1 emerges as a predictive biomarker for response to MAPKi therapy, suggesting that tumors with low AMBRA1 expression may exhibit intrinsic resistance. Second, targeting FAK1, either as monotherapy in AMBRA1^{LOW} tumors or in combination with MAPKi in AMBRA1-proficient tumors, holds therapeutic potential. The latter approach aims to prevent the selection of preexisting AMBRA1^{LOW} clones during prolonged drug exposure, thus providing a strategy to overcome the establishment of BRAFi-resistant phenotypes (Fig. 8).

In conclusion, this study proposes that a reduction in melanoma AMBRA1 expression levels evokes MAPKi-induced resistance through activation of FAK1 providing a rationale for FAKi utilization, either as monotherapy or combined therapy with MAPKi.

Materials and Methods

Human and Murine Melanoma Cell Lines. The human BRAF^{V600E}-mutated FM-93/2 [ESTDAB (European Searchable Tumor Line Database)-033], M17 (ESTDAB-039), M88 (ESTDAB-135), Ma-Mel-51 (ESTDAB-196), FM-55/M2 (ESTDAB-013), M24 (ESTDAB-043), Mel-5392 (ESTDAB-114), and OCM-3 (ESTDAB-129) cell lines were already in house and cultivated in RPMI 1640 Medium (ThermoFisher Scientific; cat#61870-010). Apart from Ma-Mel-51 and FM-55/M2, all cell lines were characterized in a previous study for expression levels of AMBRA1 (25). BRAF mutational status was previously determined (43). The human melanoma cell line SK-Mel-5 from ATCC® (Manassas) was cultivated in Advanced Minimum Essential Media (MEM) (ThermoFisher Scientific; cat#12492-021) and BRAF mutational status determined using the Cellosaurus Database. Immortalized murine melanoma cells YUMM1.7 and YUMM1.1 were previously described (44) and cultivated in DMEM (ThermoFisher Scientific; cat#31966-021). Primary Bdmc cells were generated from either BPA$^{+/+}$ (Bdmc$^{+/+}$) or BPA$^{-/-}$ (Bdmc$^{-/-}$) mice, as previously described (25) (*SI Appendix*, Fig. S3*E*) and cultivated in RPMI. Cell culture media were supplemented with 2 mM GlutaMAX™ (ThermoFisher Scientific; cat#35050-038), 100 U/mL P/S (Penicillin-Streptomycin, ThermoFisher Scientific; cat#15140-122), 1% MEM nonessential amino acids (YUMM1.1; ThermoFisher Scientific; cat#11140-050) and 7% (YUMM1.7), 20% (Bdmc), or 10% (all remaining cells) FBS (ThermoFisher Scientific; cat#10270-106) and cultivated at 37 °C in a 5% CO_2 atmosphere. During the experiments, cells were counted using Dual-Chamber Cell Counting Slides (Bio-Rad Laboratories; cat#1450011) on a TC10™ Automated Cell Counter (Bio-Rad Laboratories) and plated at a density of 1 × 10^5 cells/mL, unless otherwise indicated.

Transfection Methods. The reverse method was employed for siRNA transfection. Silencing was performed for 96 to 120 h, unless otherwise indicated. Sequences and final concentrations for custom-designed siRNAs are in *SI Appendix*, Table S1. DNA constructs for myc-flagged-AMBRA1 (myc-AMBRA1^{WT}/^{P170S}) (29), AMBRA1 (AMBRA1^{WT}/^{LIRaa}) (45), and HA-tagged-FAK1 (FAK1^{WT}/^{AA}) (25) were originated as described in the relevant references. Plasmids encoding for FAK1^{WT}/^{AA} were modified to specifically introduce silent mutations within their sequence targeted by siFAK1 and restrict the silencing effect on endogenous FAK1 only. Myc-ß-Gal-, ß-Gal, and HA-expressing plasmids were used as negative controls. All transfections were performed using Lipofectamine™ 2000 Transfection Reagent (ThermoFisher Scientific; cat#11668-019), according to the instructions.

Drugs and Treatments. The BRAFi vemurafenib (Selleckchem, cat#S1267) and dabrafenib (Selleckchem, cat#S2807) were respectively used for human and murine cell lines. The MEKi trametinib (Selleckchem, cat#S2673) was used for both human and murine cell lines. The FAKi defactinib (Selleckchem, cat#S7654) was used for both human and murine cell lines, while PF-562271 (Selleckchem, cat#S2890) only for murine cells. All drugs were dissolved in dimethyl sulfoxide (DMSO), used as vehicle in the relevant control cases. For single-dose treatments, timing and dosage were chosen either following dose-dependent experiments or to obtain a treatment efficacy ≥50% in the desired treatment group.

Generation of Resistant Cell Lines. Resistant cell lines to BRAFi were generated from pools of cells to maintain heterogeneity. 1 × 10^6 cells were separately plated and each resistant cell line (R + number, e.g., R1, R2) independently originated from its parental after exposure to 1 μM BRAFi in growth medium (conditioned medium). A control cell line (S) was kept during the selection process and treated with DMSO. Cells were defined resistant when they started to growth exponentially. Resistant cells are cultivated in conditioned medium, unless otherwise indicated.

Single-Cell-Derived Clones. Human FM-93/2 and murine YUMM1.7 cell lines were washed in PBS and detached with trypsin. Cells were centrifuged at 800 × g for 5 min, resuspended in growth medium, filtered using a 40 μm Falcon® Cell Strainer (Corning; cat#431750), diluted to a concentration of 1,000 cells/mL, single-cell sorted using a BD FACSMelody™ Cell Sorter (BD Biosciences) machine and plated in 96-well plates. 60% of clones survived and cells were allowed to fully recover before any treatment or further analysis.

Cell Viability. 5,000 cells were plated in triplicates in 96-well plates and treated after 24 h. Percentage of cell viability and EC_{50} values were determined by the Cell Counting Kit-8 (Dojindo; cat#CK04-11) as previously described (25). Resistance indexes to BRAFi and MEKi (MAPKi) were calculated as the ratio between percentage of survival of MAPKi-treated and -untreated cells. Response to FAKi in cotreatment experiments was calculated as the reverse ratio between a FAKi treatment case and its relevant control, as follows: $[(BRAFi+FAKi)/BRAFi]^{-1}$ and $(FAKi/Vehicle)^{-1}$.

Colony Formation Assay. First, 16 cells/cm^2 were plated in 6-well plates and treated after 24 h with BRAFi (vemurafenib 250 nM) and/or FAKi (defactinib 500 nM) for 3 wk. Then, cells were fixed and stained with 0.05% (w/v) Crystal Violet in 20% MeOH. Plates were imaged and colonies counted manually. The percentage of surviving colonies was calculated as the ratio between the number of colonies in the treated groups vs. the control case.

Transwell Migration assay. 1 × 10^4 M17 and YUMM1.7 (S, R1, and R2) cells were seeded in Nunc™ Polycarbonate Cell Culture Inserts (ThermoFisher Scientific; cat#140629) as previously described (25). Cells were cultured for 24 h and nuclei of cells migrated to the bottom counterstained with 1 μg/mL Hoechst 33342 (ThermoFisher Scientific; cat#H3570) for 10 min at RT. Images were captured with a Celigo Image Cytometer (Nexcelom Bioscience). Twenty-five separate fields were acquired, and nuclei counted using the Celigo Image Cytometer Analysis Software. Fluorescence images were adjusted for brightness, contrast, and color balance using Fiji analysis software.

Immunofluorescence Analysis. A total of 3 × 10^5 FM-93/2 S, R1, and R2 cells were seeded in duplicates in Ibidi 8-wells (Ibidi 80826, ibiTreat), incubated for 24 h, fixated in −20 °C MeOH for 10 min, washed in PBS, blocked in 1% bovine serum albumine (BSA) in PBS for 30 min and incubated with anti-AMBRA1 primary antibody (1:100) in a humidity chamber at 4 °C O/N. Secondary antibody was added 1:1,000 in 1% BSA and incubated in a dark box at RT for 1 h. Nuclei were counterstained with DAPI (Invitrogen™, cat#R37606). Samples were imaged with a Nikon Eclipse Ti2 Widefield using a 20× air objective and images analyzed using Nikon's analysis software. Analysis was made based on maximum intensity projections of Z-stacks. The mean object intensity from the maximum projection of AMBRA1 signal was then measured in each segmentation and visualized in a plot. Further details are provided in *SI Appendix*.

PI Staining. At the experimental endpoint, both adherent and in-suspension cells were collected and centrifuged at 2,000 × g for 5 min at RT, followed by a wash with PBS. Cell pellets were resuspended in PI staining solution (50 μg/mL PI, 0.1% sodium citrate, 0.1% Triton X-100, 200 μg/mL RNAse) for 30 min at 4 °C in the dark. Fluorescence intensity was analyzed in logarithmic scale using a BD FACSVerse™ Cell Analyzer (BD Biosciences) machine. Raw data were analyzed with the FlowJo v.10.6.1 software and dead cells expressed as fold change of sub-G1 cells vs. control case.

Subcutaneous Injections and In Vivo Treatments. Subcutaneous injection of either Bdmc$^{+/+}$ (sBPA$^{+/+}$ mice) or Bdmc$^{-/-}$ (sBPA$^{-/-}$ mice) cells (2 × 10^6/mouse) was performed in female C57Bl/6 N mice (Taconic Biosciences A/S; 10 to 12 wk of age) as previously described (25). When tumors were measurable, mice were randomly divided into subgroups and treated. Drugs were dissolved in DMSO, freshly diluted in Hydroxypropyl methylcellulose and 0.2% Tween®80 (HPMT) at a final dosage of 30 mg/kg dabrafenib and 50 mg/kg PF-562271 and P.O. administered for 21 d, including (Fig. 3 *J–L*) or excluding (*SI Appendix*, Fig. S6*H*) weekends. Control mice were administered a HPMT+DMSO solution. Tumors were measured using a digital caliper in width and length and volumes (V) determined using the formula $V = (a \times b^2)/2$, where $a > b$. Alternatively, tumor weights were measured when the mice were killed.

Protein Expression Analysis. Cells were washed in PBS, collected, and centrifuged at 800 × g for 5 min at RT. Cell lines and tumor samples were processed and total protein lysates obtained as previously described (25). For detection of pFAK-Y397, cells were directly disrupted in cell plates after plates were washed and fully dried of PBS. Samples were separated by sodium dodecyl-sulfate polyacrylamide gel electrophoresis (SDS-PAGE) using Criterion™ TGX Stain-Free™ Precast Gels (Bio-Rad Laboratories; cat#5678084 and cat#5678085) and blotted onto 0.2 μm polyvinylidene difluoride (PVDF) membranes (Bio-Rad Laboratories; cat#1704157) using a Trans-Blot® Turbo™ Transfer System (Bio-Rad Laboratories). Primary antibodies used are listed in *SI Appendix*, Table S2. PVDF membranes were incubated with the ECL™ Prime Western Blotting Detection Reagent (Amersham; cat#RPN2236) prior to detection with a ChemiDoc™ MP System (Bio-Rad Laboratories) provided with the Image Lab 6.0.1 Software (Bio-Rad Laboratories). Proteins on gels were visualized and an image captured before gels were blotted (Stain-Free activation). Densitometry analyses were performed using ImageJ version 1.52.q.

RNA Isolation and qRT-PCR. Total RNA isolation and RT from both cell and tumor samples were performed as previously described (25). Expression levels of the mRNAs of interest were measured using the PowerUp™ SYBR™ Green Master Mix (ThermoFisher Scientific; cat#A25742) on a ViiA 7 Real-Time PCR System v1.3 (Applied Biosystems). Reactions were run as triplicates and data normalized on the internal housekeeping *L34*. Custom-designed primer pairs are listed in *SI Appendix*, Table S3 and were tested through Primer-BLAST prior to purchase (TAG Copenhagen A/S).

Analyses of Publicly Available Datasets. Arbitrary cut-offs were applied to define AMBRA1^{HIGH}/^{LOW} subgroups in The Cancer Genome Atlas skin cutaneous melanoma (TCGA-SKCM) (mRNA) and the CCLE (protein) as previously described (25). Sample values for *AMBRA1* in the GSE50509 (ID = ILMN_1662681) and in the GSE65185 (Gene ID: 55626) cohorts were downloaded to subgroup pretreatment samples in AMBRA1^{HIGH}/^{LOW} and the Log_2 of the *AMBRA1* expression ratio between MAPKi-treated and matching pretreatment tumors graphed as waterfall plot. For PDXs, AMBRA1 expression was analyzed in a subset of matched PDXs before (PRE) and after (PROG) MAPKi treatment from GSE129127 (32). For single-cell quantification of AMBRA1 positive cells in melanoma PDX during different phases upon MAPKi treatment (MEL006), data were downloaded from GSE116237 (33) and analyzed as previously described (46). All GSEAs were performed as previously described (25) on the Melanocytic, Undifferentiated, NCSC-like by Tsoi et al. (37) and Invasive by Hoek et al. (38) gene signatures. For the correlation analysis between *AMBRA1* and *NGFR, AXL,* and *MITF* expression, RSEM normalized mRNA data were downloaded from TCGA-SKCM samples (n = 448) through R studio using "TCGAbiolink" package

(47). Pearson and Spearman correlations were calculated using Prism 9. Further details are provided in *SI Appendix*.

PRISM Database Analysis. To evaluate the differential cytotoxic action of a panel of BRAFi and MEKi on melanoma cell lines, the primary PRISM database (48) was utilized. The list of BRAFis and MEKis was retrieved from the Drug Repurposing Hub (49). Melanoma cell lines were classified based on their BRAF mutation status using ExPASy Bioinformatics Resource Portal. To test the link between the drug scores and the protein levels of AMBRA1, protein expression of screened cell lines was retrieved from CCLE (50). The individual drug scores on each cell line were visualized in a heatmap with cell lines sorted by AMBRA1 protein expression. To determine the association between the genes of interest and drug scores, a linear model was fitted between the median drug scores in a cell line and the protein expression of this cell line. Further details are provided in *SI Appendix*.

Statistical Analysis. Statistical analyses were performed with GraphPad Prism9. Significance was designated as follows: $*P < 0.05$; $**P < 0.01$; $***P < 0.001$; $****P < 0.0001$; ns = not significant. Data are shown as average ±SEM or SD, as indicated in the relevant figure legends. Further details are provided in *SI Appendix*.

Data, Materials, and Software Availability. The transcriptomic datasets analyzed in the current study are public available under the GEO numbers GSE50509 (30), GSE65185 (31), GSE129127 (32), and GSE116237 (33). The RNAseq datasets from the TCGA-SKCM are available at http://cancergenome.nih.gov/ (47). The protein data from the CCLE melanoma cell lines are available at portals.broadinstitute.org/ccle (50).

ACKNOWLEDGMENTS. We thank Maria Zappalà, Aline Genbauffe, Laura Gonzáles Requesón, Sofie Ewerman, and Lina Vardouli and acknowledge the Animal Facility at the Danish Cancer Institute. This study has received support from Danish Cancer Society (KBVU R204-A12424 and R352-A20515 to D.D.Z., R231-A14034 and R325-A19075 to F.C., and R146-A9414 and R231-A13855 to G.F.), Leo Foundation (LF-OC-19-000004 to D.D.Z., LF-OC-19-000219 to J.R.B), Novo Nordisk Foundation (NNF18OC0052550 and NNF22OC0079352 to G.F., and NNF21OC0070834 to F.C.), AIRC Foundation (IG2017-20719 to G.F. and IG2019- 23543 to F.C.), NEYE Foundation, Melanoma Research Alliance (MRA 620385). Immunofluorescence imaging was performed at the Danish Molecular Biomedical Imaging Center (DaMBIC, University of Southern Denmark), supported by Novo Nordisk Foundation (NNF18SA0032928 to J.R.B.). The Melanoma Research Team is part of the CARD, funded by Danmarks Grundforskningsfond (DNRF125).

Author affiliations: [a]Melanoma Research Team, Center for Autophagy, Recycling and Disease, Danish Cancer Institute, Copenhagen 2100, Denmark; [b]Department of Life Sciences and Medicine, University of Luxembourg, Belvaux 4365, Luxembourg; [c]Redox Biology Group, Danish Cancer Institute, Copenhagen 2100, Denmark; [d]Molecular Diagnostics Group, Danish Cancer Institute, Copenhagen 2100, Denmark; [e]Department of Biochemistry and Molecular Biology, University of Southern Denmark, Odense 5230, Denmark; [f]Department of Pathology, New York University Grossman School of Medicine, New York, NY 10016; [g]Cell Stress and Survival, Center for Autophagy, Recycling and Disease, Danish Cancer Institute, Copenhagen 2100, Denmark; [h]Faculty of Medicine and Surgery, Università Cattolica del "Sacro Cuore", Fondazione Policlinico Gemelli—Istituti di Ricovero e Cura a Carattere Scientifico (IRCCS), Rome 00136, Italy; [i]Université Côte d'Azur, Nice 06200, France; [j]Inserm, Biology and Pathologies of melanocytes, team1, Equipe labellisée Ligue 2020, Centre Méditerranéen de Médecine Moléculaire, Nice 06200, France; [k]Department of Cancer and Inflammation Research, Institute of Molecular Medicine, University of Southern Denmark, Odense 5230, Denmark; [l]Department of Oncology, Odense University Hospital, Odense 5000, Denmark; and [m]Translational and Clinical Research Institute, Medical School, Newcastle University, Newcastle upon Tyne NE2 4HH, United Kingdom

1. G. V. Long, S. M. Swetter, A. M. Menzies, J. E. Gershenwald, R. A. Scolyer, Cutaneous melanoma. *Lancet* **402**, 485–502 (2023).
2. A. H. Shain, B. C. Bastian, From melanocytes to melanomas. *Nat. Rev. Cancer* **16**, 345–358 (2016).
3. A. H. Shain *et al.*, Genomic and transcriptomic analysis reveals incremental disruption of key signaling pathways during melanoma evolution. *Cancer Cell* **34**, 45–55.e4 (2018).
4. P. A. Ascierto *et al.*, Cobimetinib combined with vemurafenib in advanced BRAF(V600)-mutant melanoma (coBRIM): Updated efficacy results from a randomised, double-blind, phase 3 trial. *Lancet Oncol.* **17**, 1248–1260 (2016).
5. P. B. Chapman *et al.*, Improved survival with vemurafenib in melanoma with BRAF V600E mutation. *N. Engl. J. Med.* **364**, 2507–2516 (2011).
6. R. Dummer *et al.*, Encorafenib plus binimetinib versus vemurafenib or encorafenib in patients with BRAF-mutant melanoma (COLUMBUS): A multicentre, open-label, randomised phase 3 trial. *Lancet Oncol.* **19**, 603–615 (2018).
7. A. Hauschild *et al.*, Dabrafenib in BRAF-mutated metastatic melanoma: A multicentre, open-label, phase 3 randomised controlled trial. *Lancet* **380**, 358–365 (2012).
8. R. W. Jenkins, D. E. Fisher, Treatment of advanced melanoma in 2020 and beyond. *J. Invest. Dermatol.* **141**, 23–31 (2021).
9. J. Larkin *et al.*, Combined vemurafenib and cobimetinib in BRAF-mutated melanoma. *N. Engl. J. Med.* **371**, 1867–1876 (2014).
10. C. Robert *et al.*, Improved overall survival in melanoma with combined dabrafenib and trametinib. *N. Engl. J. Med.* **372**, 30–39 (2015).
11. B. Domingues, J. M. Lopes, P. Soares, H. Populo, Melanoma treatment in review. *Immunotargets Ther.* **7**, 35–49 (2018).
12. J. J. Luke, K. T. Flaherty, A. Ribas, G. V. Long, Targeted agents and immunotherapies: Optimizing outcomes in melanoma. *Nat. Rev. Clin. Oncol.* **14**, 463–482 (2017).
13. S. Y. Lim, A. M. Menzies, H. Rizos, Mechanisms and strategies to overcome resistance to molecularly targeted therapy for melanoma. *Cancer* **123**, 2118–2129 (2017).
14. O. Marin-Bejar *et al.*, Evolutionary predictability of genetic versus nongenetic resistance to anticancer drugs in melanoma. *Cancer Cell* **39**, 1135–1149.e8 (2021).
15. D. Hanahan, Hallmarks of cancer: New dimensions. *Cancer Discov.* **12**, 31–46 (2022).
16. I. Arozarena, C. Wellbrock, Phenotype plasticity as enabler of melanoma progression and therapy resistance. *Nat. Rev. Cancer* **19**, 377–391 (2019).
17. M. Fallahi-Sichani *et al.*, Adaptive resistance of melanoma cells to RAF inhibition via reversible induction of a slowly dividing de-differentiated state. *Mol. Syst. Biol.* **13**, 905 (2017).
18. C. Pagliuca, L. Di Leo, D. De Zio, New insights into the phenotype switching of melanoma. *Cancers (Basel)* **14**, 6118 (2022).
19. F. Rambow, J. C. Marine, C. R. Goding, Melanoma plasticity and phenotypic diversity: Therapeutic barriers and opportunities. *Genes Dev.* **33**, 1295–1318 (2019).
20. V. Cianfanelli *et al.*, Ambra1 at a glance. *J. Cell Sci.* **128**, 2003–2008 (2015).
21. G. M. Fimia *et al.*, Ambra1 regulates autophagy and development of the nervous system. *Nature* **447**, 1121–1125 (2007).
22. A. C. Chaikovsky *et al.*, The AMBRA1 E3 ligase adaptor regulates the stability of cyclin D. *Nature* **592**, 794–798 (2021).
23. V. Cianfanelli *et al.*, AMBRA1 links autophagy to cell proliferation and tumorigenesis by promoting c-Myc dephosphorylation and degradation. *Nat. Cell Biol.* **17**, 20–30 (2015).
24. I. Cosgarea *et al.*, Melanoma secretion of transforming growth factor-beta2 leads to loss of epidermal AMBRA1 threatening epidermal integrity and facilitating tumour ulceration. *Br. J. Dermatol.* **186**, 694–704 (2022).
25. L. Di Leo *et al.*, Loss of Ambra1 promotes melanoma growth and invasion. *Nat. Commun.* **12**, 2550 (2021).
26. E. Maiani *et al.*, AMBRA1 regulates cyclin D to guard S-phase entry and genomic integrity. *Nature* **592**, 799–803 (2021).
27. D. Simoneschi *et al.*, CRL4(AMBRA1) is a master regulator of D-type cyclins. *Nature* **592**, 789–793 (2021).
28. A. Frias *et al.*, Ambra1 modulates the tumor immune microenvironment and response to PD-1 blockade in melanoma. *J. Immunother. Cancer* **11**, e006389 (2023).
29. M. Tiberti *et al.*, The Cancermuts software package for the prioritization of missense cancer variants: A case study of AMBRA1 in melanoma. *Cell Death Dis.* **13**, 872 (2022).
30. H. Rizos *et al.*, BRAF inhibitor resistance mechanisms in metastatic melanoma: Spectrum and clinical impact. *Clin. Cancer Res.* **20**, 1965–1977 (2014).
31. W. Hugo *et al.*, Non-genomic and immune evolution of melanoma acquiring MAPKi resistance. *Cell* **162**, 1271–1285 (2015).
32. J. Boshuizen *et al.*, Reversal of pre-existing NGFR-driven tumor and immune therapy resistance. *Nat. Commun.* **11**, 3946 (2020).
33. F. Rambow *et al.*, Toward minimal residual disease-directed therapy in melanoma. *Cell* **174**, 843–855.e19 (2018).
34. K. S. Hoek *et al.*, In vivo switching of human melanoma cells between proliferative and invasive states. *Cancer Res.* **68**, 650–656 (2008).
35. K. S. Hoek, C. R. Goding, Cancer stem cells versus phenotype-switching in melanoma. *Pigm. Cell Melanoma Res.* **23**, 746–759 (2010).
36. I. Kozar, C. Margue, S. Rothengatter, C. Haan, S. Kreis, Many ways to resistance: How melanoma cells evade targeted therapies. *Biochim. Biophys. Acta Rev. Cancer* **1871**, 313–322 (2019).
37. J. Tsoi *et al.*, Multi-stage differentiation defines melanoma subtypes with differential vulnerability to drug-induced iron-dependent oxidative stress. *Cancer Cell* **33**, 890–904.e5 (2018).
38. K. S. Hoek *et al.*, Metastatic potential of melanomas defined by specific gene expression profiles with no BRAF signature. *Pigm. Cell Res.* **19**, 290–302 (2006).
39. H. Davies *et al.*, Mutations of the BRAF gene in human cancer. *Nature* **417**, 949–954 (2002).
40. F. Spagnolo, P. Ghiorzo, P. Queirolo, Overcoming resistance to BRAF inhibition in BRAF-mutated metastatic melanoma. *Oncotarget* **5**, 10206–10221 (2014).
41. D. Perna *et al.*, BRAF inhibitor resistance mediated by the AKT pathway in an oncogenic BRAF mouse melanoma model. *Proc. Natl. Acad. Sci. U.S.A.* **112**, E536–545 (2015).
42. E. Hirata *et al.*, Intravital imaging reveals how BRAF inhibition generates drug-tolerant microenvironments with high integrin beta1/FAK signaling. *Cancer Cell* **27**, 574–588 (2015).
43. C. Dahl *et al.*, Mutual exclusivity analysis of genetic and epigenetic drivers in melanoma identifies a link between p14 ARF and RARbeta signaling. *Mol Cancer Res.* **11**, 1166–1178 (2013).
44. K. Meeth, J. X. Wang, G. Micevic, W. Damsky, M. W. Bosenberg, The YUMM lines: A series of congenic mouse melanoma cell lines with defined genetic alterations. *Pigm. Cell Melanoma Res.* **29**, 590–597 (2016).
45. F. Strappazzon *et al.*, AMBRA1 is able to induce mitophagy via LC3 binding, regardless of PARKIN and p62/SQSTM1. *Cell Death Differ.* **22**, 419–432 (2015).
46. P. Berico *et al.*, CDK7 and MITF repress a transcription program involved in survival and drug tolerance in melanoma. *EMBO Rep.* **22**, e51683 (2021).
47. A. Colaprico *et al.*, TCGAbiolinks: An R/Bioconductor package for integrative analysis of TCGA data. *Nucleic Acids Res.* **44**, e71 (2016).
48. S. M. Corsello *et al.*, Discovering the anti-cancer potential of non-oncology drugs by systematic viability profiling. *Nat. Cancer* **1**, 235–248 (2020).
49. S. M. Corsello *et al.*, The drug repurposing hub: A next-generation drug library and information resource. *Nat. Med.* **23**, 405–408 (2017).
50. D. P. Nusinow *et al.*, Quantitative proteomics of the cancer cell line encyclopedia. *Cell* **180**, 387–402. e16 (2020).